NASA Technical Memorandum 106435
AIAA–94–0865

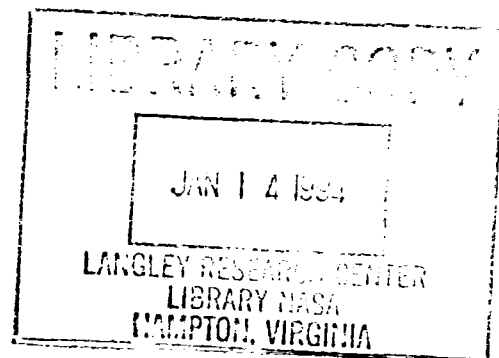# Comparison of Mixing Calculations for Reacting and Non-reacting Flows in a Cylindrical Duct

V.L. Oechsle and H.C. Mongia
Allison Gas Turbine Division
General Motors Corporation
Indianapolis, Indiana

and

J.D. Holdeman
National Aeronautics and Space Administration
Lewis Research Center
Cleveland, Ohio

NASA

COMPARISON OF MIXING CALCULATIONS FOR REACTING AND NON-REACTING FLOWS IN A CYLINDRICAL DUCT

V. L. Oechsle* and H. C. Mongia*
Allison Gas Turbine Division
General Motors Corporation
Indianapolis, In 46206

J. D. Holdeman§
National Aeronautics and Space Administration
Lewis Research Center
Cleveland, OH 44135

Abstract

A production 3-D elliptic flow code has been used to calculate non-reacting and reacting flow fields in an experimental mixing section relevant to a rich-burn/quick-mix/lean-burn (RQL) combustion system. A number of test cases have been run to assess the effects of the variation in the number of orifices, mass flow ratio and rich-zone equivalence ratio on the flow field and mixing rates. The calculated normalized temperature profiles for the non-reacting flow field agree qualitatively well with the normalized conserved variable isopleths for the reacting flow field indicating that non-reacting mixing experiments are appropriate for screening and ranking potential rapid mixing concepts. For a given set of jet momentum-flux ratio, mass flow ratio, and density ratio (J, MR, and DR), the reacting flow calculations show a reduced level of mixing compared to the non-reacting cases. In addition, the rich-zone equivalence ratio has noticeable effect on the mixing flow characteristics for reacting flows.

Nomenclature

A   area
A_m duct crossectional area, also A_{tot}, m^2
ACd also A_j, effective orifice area m^2

* AIAA member
§ Senior Research Engineer, AIAA Associate Fellow

Ar	area ratio (jet/mainstream) = $A_j/A_m = ACd/A_m$
AMIX	area weighted overall T or ϕ deviation from equilibrium, Eq 3
AHOT	area weighted T or ϕ deviation above equilibrium, Eq 4
ACOLD	area weighted T or ϕ deviation below equilibrium, Eq 5
B	area determined half width of the distribution function
C	constant of proportionality between $\sqrt{J}$ and S/R, Eq-9
d	diameter of the orifice
DR	density ratio (jet/mainstream)
DP/P	total pressure loss across the mixing wall, %
f	non-dimensional temperature and/or equivalence ratio, Eq 2
f/a	fuel to air ratio
j	radial vector direction
J	momentum-flux ratio (jet/mainstream) = M^2/DR, also $(MR)^2/[(DR)(A_j/A_m)^2]$
k	tangential vector direction
m_{tot}	overall mixer mass flowrate, kg/sec = $m_{jet} + m_{main}$
M	mass flux ratio (jet/mainstream) = DR V_{jet}/U_{main}
MMIX	mass flow weighted overall T or ϕ deviation from equilibrium, Eq 6
MHOT	mass flow weighted T or ϕ deviation above equilibrium, Eq-7
MCOLD	mass flow weighted T or ϕ deviation below equilibrium, Eq-8
MR	mass flowrate ratio (jet/mainstream)
n	optimum number of orifices / row, Eq-9
P	total pressure, atm.
R	radius of the mixing section, m

r	radial distance from the centerline of the mixer, m
S	orifice spacing in the circumferential direction
T	temperature, K
u	local axial velocity, m/sec
U_{main}	approach mainstream axial velocity, m/sec
VR	velocity ratio (jet/mainstream) $= V_{jet} / U_{main}$
V_{jet}	radial velocity of the jet, m/sec
w	jet width, m, see Fig-3
x	axial distance from the leading edge of the orifice
α	parameter used in Eq-2 through 8, can be either temperature or equivalence ratio
δ	value of the cumulative volume fraction at the fequil , Fig-4
ρ	fluid density, kg/m^3
ϕ	equivalence ratio $(f/a)_{local} / (f/a)_{stoi}$

Subscripts

equil	equilibrium
j	jet
m	mainstream, also (main)
RZ	rich-zone
stoi	stoichiometric

Introduction

Advanced fuel-efficient commercial turbo propulsion gas turbines pose a number of design challenges for combustion systems including durability, aerothermal performance, wide operability range, and exhaust emissions. Conventional gas turbine combustion system employs a single stage combustion zone which has been optimized to produce low exhaust emissions of carbon monoxide, and unburned hydrocarbons at idle and near-idle operating conditions. Exhaust smoke below the threshold of plume visibility throughout the engine operation range has also been maintained without adversely affecting engine starting, stability, and relight requirement. Moderate reductions in NO_x emissions (up to 30%) have been achieved in single-combustion-zone combustors by reducing unmixedness and combustion zone residence time. Further reductions in high-power NO_x emissions (e.g. up to 50% from state-of-the-art levels) would require design and development of two-stage combustion concepts including radially or axially staged combustion zones. These types of combustion systems are currently under development.

In order to achieve more demanding (70 to 90%) NO_x reduction goals of the advanced turbine engines which will also have considerably higher overall pressure ratios and turbine rotor inlet temperatures, significant advances are needed in the design and development of combustion systems employing multi-staging concepts including lean premix (LPP) and rich burn/quick mix/lean burn (RQL) (Shaw, 1991). The RQL concept studied in-depth by Rizk and Mongia (e.g. Rizk

and Mongia, 1990; 1991; 1993) appears to have a number of advantages over other competing ultra-low NO_x concepts provided one can significantly enhance the mixing during the transition from rich to lean-side combustion. Additional experimental and analytical research effort (e.g. Howe., et al., 1991; Smith, Talpallikar, and Holdeman, 1991; Talpallikar et al., 1991; Vranos et al., 1991; Bain, Smith, and Holdeman, 1992, 1993; Liscinsky et al., 1992; Zhu and Lai, 1992; Doerr and Hennecke, 1993; Liscinsky, True, and Holdeman, 1993) is underway to study and identify the critical design and flow parameters affecting the mixing effectiveness.

An integrated analytical and experimental investigation between the authors and the UCI Combustion Laboratory has been underway to quantify non-reacting mixing processes in a 80 mm diameter cylindrical test section, as summarized by Hatch et al., 1992, Kroll et al., 1993, and Oechsle, Mongia, and Holdeman, 1992, 1993. These studies have shown that the mixing section effectiveness is affected by the jet-to-mainstream momentum-flux ratio (J), mass flow ratio (MR), and orifice/slot design parameters including R/d, and S/d, aspect ratio and slot orientation. Here R, d, and S are the radius of the mixing section, orifice diameter, and circumferential spacing between the orifice centers, respectively. The qualitative agreement between predictions and measurements is reasonably good, and the model calculations can be used to provide further insight especially for the flow variables that have not been measured.

A logical question that could be raised is: are the non-reacting mixing investigations appropriate for defining an optimum mixer geometry. This paper summarizes the results of a parallel study to compare the mixing performance of an RQL mixing section in both reacting and non-reacting environments using constant main flow parameters such as jet-to-mainstream momentum-flux ratio (J), mass flow ratio (MR), and density ratio (DR) and establish the difference in the flow field structure. In this study, the mixing effectiveness of a jet in a crossflow is numerically investigated using a 3-D analytical code. Eight different circular orifice configurations were analyzed in a cylindrical mixing section at J=25 with both 8 and 12 orifices per row. The reacting flow configurations were calculated with mainstream incoming species mole fractions simulating reacting rich-zone equivalent ratios of 1.35 and 1.80. The procedure used to model the geometric configurations was similar to that used by Oechsle, Mongia, and Holdeman, 1992, 1993.

Mathematical Model

A production 3-D combustor code, COM-3D (Bruce, Mongia, and Reynolds, 1979) is used that solves the turbulent reacting flow transport equations using the SIMPLE algorithm of Patankar and Spalding (Patankar, 1980). This program simulates turbulence by the two-equation k-ε model (Launder and Spalding, 1974), and combustion following vaporization is determined by a four-step chemical reaction

model based on Arrhenius and modified eddy breakup concepts. The transport equations for all dependent variables are of the following form as shown in Eq-1:

$$\text{div}[\rho_r u \xi - (\mu_{eff}/P_r) \text{ grad}(\xi)] = S_\xi \qquad (1)$$

where ρ_r is the mixture density, u is the velocity, μ_{eff} is the effective turbulent viscosity, P_r is the effective Prandtl/Schmidt number, and S_ξ is the source term for the variable ξ. The following variables are computed by COM-3D: 1) axial, radial, and swirl velocity components; 2) specific enthalpy and temperature; 3) turbulence kinetic energy and dissipation rate; 4) unburned fuel, CO, H_2, intermediate fuel, and composite fuel mass fractions; and 5) fuel spray trajectory and evaporation rate.

The computational effort is significantly reduced by modeling a sector of the mixing section comprising a single orifice. Therefore, the shape of the sector was dependent on the number of orifices equally spaced in the circumferential direction. It should be noted that 8 orifices/row yield a computational domain of a 45 degree sector, and similarly, 12 orifices/row yield a 30 degree sector. Periodic boundary conditions were applied in the circumferential direction. No-slip and adiabatic boundary conditions were applied at the outer wall defining the inside wall of the mixing section. Zero-gradient boundary conditions were applied at the center axis. Axial gradients at the exit boundary condition were assumed zero.

Geometric Configuration

In this study, the mixing section was modeled as a constant diameter cylindrical duct with a single row of equally spaced orifices. The outer wall diameter is 80 mm and the axial length of the mixing section extended from x/R=-1.4 to x/R=6 where x is referenced from the leading edge of the orifice. Sufficient axial distance was provided both upstream and downstream of the orifice to minimize the impact of the inlet and exit boundary conditions on the calculated flow structure in the primary domain of interest which is 0<x/R<1. The computational grid domain was typically discretized into 50,000 to 80,000 finite control volumes. The grid was typically denser near the orifice and near the outer wall to resolve the high velocity and temperature gradients resulting from the inlet of the crossflow jet. An orthogonal view of a typical grid arrangement is shown in Figure-1. The grid is normally configured to allow smooth progressive volume change between adjacent control volumes to help speed up the convergence of the solution.

The geometric configurations of the jet orifices is also shown in Figure-1. A total of 8 circular hole configurations were analyzed. Also, it should be noted that the normalized temperature, normalized equivalence ratio, and velocity profile plots shown in this paper depict plane sections in a) the

axial-radial plane through the center of the jet from x/R=-0.5 to x/R=2.5, and b) the radial-tangential plane at x/R=1 (one full mixer radius downstream from the leading edge of the jet). The axial, radial, and tangential directions are shown in Figure-1. It should be noted that the flow direction is from left-to-right in the axial-radial planes and into the paper for the radial-tangential planes.

The overall description of the eight configurations is given in Table-1 and Figure-2. Cases 1, 3, 5, and 7 are for non-reacting flows and the corresponding reacting flow cases are denoted by 2, 4, 6, and 8, respectively. It is assumed that practical RQL mixing sections will have liner pressure drop and J approximately 3% of P_{main} and 25, respectively. The rich-zone equivalence ratio is assumed to lie between 1.35 and 1.80 and lean-zone equivalence ratio is typically 0.45. It is also assumed that the non-reacting experiment is performed at atmospheric pressure whereas the reacting experiment might be run at high inlet temperature and pressure conditions. It is further assumed that both reacting and non-reacting experiments will be conducted with comparable values of J, mass flow ratio (MR), density ratio (DR), area ratio (Ar), and quick mix section liner pressure drop (DP/P).

The eight cases that have been run are for fixed values of J=25; MR=1.83 and 2.67; corresponding to rich-zone equivalence ratio, ϕ_{RZ}=1.35 and 1.80, and other variables listed in Table-1. The blockage is defined as the circumferential projection of the orifice divided by the spacing between the orifice centers. Typically 150 to 200 finite control volume nodes were used to simulate the orifice.

The reacting flow conditions, the operating pressure and temperature simulated realistic gas turbine operating conditions (P= 13.4 atm., T= 978K). The mainstream flow and jet flow conditions are show in Table-1. The incoming mainstream species mole fractions for (CO, CO_2, H_2O, and H_2) were determined based on the given rich-zone equivalence ratio (see Table-1) at equilibrium at the prescribed operating conditions using JP-5 for the typical fuel properties. Although this assumption may not be totally realistic in an operating RQL rich section, it does provide a baseline for comparison. It is recognized that the rich-zone will produce a great amount of CO and unburned hydrocarbons which are directly admitted to the mixing region. This will probably increase the reaction in the mixing zone prompted by the mixture with the additional air. However, since the rich-zone performance greatly depends on the residence time and geometric parameters, and since its design is not within the scope of this study, the assumed rich-zone performance (achieving chemical equilibrium) is a reasonable initial condition towards analyzing the reaction in the mixing zone. The four specified species used in the inlet mainstream condition correspond to the four-step chemical reaction used in COM-3D. The species mole fractions, temperature, and velocity profiles were assumed to be uniform across the inlet cross-section of the mixing section. The jet-to-mainsteam mass flow ratio was determined by the prescribed lean zone

3

equivalence ratio of 0.45 (which is constant for all reacting flow configurations reported herein). The air jet flow was characterized by a radial, uniform flow across the orifice effective area. The assumption of uniform mass injection/area is applied in the mathematical model in all the analyzed configurations.

The non-reacting configuration models were setup for typical atmospheric temperature and pressure conditions (T_{jet} = 300K, P=1 atm.) for which the mainstream inlet flowrate was varied to obtain the same J, MR, DR, orifice ACd, and DP/P as the comparable reacting flow case. Note that in the actual optimization process, slight variations in the density ratio were obtained as shown in Table-1.

The turbulence kinetic energy of the mainstream and jet flows were 0.3% of the square of the mean velocities. The turbulence length scales of the mainstream flow were 2% of the mixer diameter, and the turbulence length scale of the jet was of the order of the orifice diameter. The inlet conditions for all orifices in the mixing section were equal to create a symmetrical input condition about the circumferential direction which was necessary for the sector analysis.
A typical numerical solution took about 250 iterations for full convergence with overall mass flow residuals of 0.05% of the total mixing section mass flowrate. All solutions were obtained using the Cray Y-MP and a typically converged solution took about 1 to 1.5 hrs of CPU time. The reacting flow solutions consumed about twice the CPU time due to the additional species variables which are solved in the model.

Results and Discussion

The mixing performance for all configurations analyzed in this study were ultimately evaluated at x/R =1. It is however recognized that the mixing performance throughout the mixing section volume of interest (0≤x/R≤1) should also be considered since complex structures are present in the flow field especially near the entry of the jet.
Two different methods were used to analyze the numerical results:

1) the results were analyzed qualitatively by visual observation of the temperature, equivalence ratio, and velocity field solutions. The temperature and equivalence ratio results are presented as normalized values with respect to the overall differential between the mainstream flow and the jet flow inlet temperatures and equivalence ratios consecutively. This normalized parameter (f) is defined in Eq-2 where α = temperature or equivalence ratio.

$$f = \frac{\alpha_{jk} - \alpha_{jet}}{\alpha_{main} - \alpha_{jet}} \qquad (2)$$

The value of (f) varies from 0 to 1, where 0 is the value of the unmixed jet and 1 is the value of the mainstream flow. Note that f = 1-θ, where θ is as defined previously (Holdeman, 1993) and used elsewhere also. It is also important to note that the definition of (f) also applied for the normalized equivalence ratio in the reacting flow configurations where f=1 equals the rich-zone equivalence ratio and f=0 is the jet equivalence ratio. The definition of (f) however does not apply to the temperature distribution in the reacting flow solutions since the temperature in some areas of the mixing region rise above that of the incoming mainstream flow due to the chemical reaction of the rich-zone exit composition. The value of the equilibrium temperature (as applied to the non-reacting conditions) and equilibrium equivalence ratio (applied to the reacting conditions) based on the normalized definition parameter (f) in Eq-1 are also equivalent since both are conserved variables. Both equilibrium values were calculated in a purely adiabatic system at any location downstream of the jet injection.

In addition to the temperature and equivalence ratio distribution plots, the velocity plots in the axial-radial plane through the orifice center are shown for all configurations for x/R from -0.5 to 2.5. In each plot, the streamlines corresponding to the developing jet in the mixing section are shown depicting the jet penetration and jet width. The values of the jet width (w) and mean jet penetration evaluated at x/R= 0.625, 1, and 2 are tabulated in Table-2 and the pictorial definition of both of these parameters is shown in Figure-3. The jet penetration at x/R=2 is shown only for the purpose to establish if complete penetration is obtained at x/R=1.

2) Three different statistical methods are reported in this paper:

a) The performance of the mixing section at the radial-tangential planes at x/R=1 was quantified by using area weighted planar deviation parameters. The smallest deviation indicates the best mixing configuration. Three different parameters (mixing deviations) AMIX, AHOT, and ACOLD are described in Eq-3 through Eq-5. Note that AMIX also equals the square root of the sum of the squared values of both AHOT and ACOLD. It is also important to note that the definitions in Eq-3 through Eq-5 do not correct the mixing non-uniformity for the bias introduced in the region of the section where the air is being injected through the orifice. This is accepted since the comparison between the reacting and non-reacting results is only performed at x/R=1 which is downstream of the trailing edge of all orifices. The area-weighted non-uniformity results are shown in Table-3.

$$AMIX = \left[\frac{1}{A_{tot}} \sum_{jk} A_{jk} \left[\frac{\alpha_{jk} - \alpha_{eq}}{\alpha_{main} - \alpha_{jet}} \right]^2 \right]^{1/2} \qquad (3)$$

$$AHOT = \left[\frac{1}{A_{tot}} \sum_{jk} A_{jk} \left[\frac{\alpha_{jk} - \alpha_{eq}}{\alpha_{main} - \alpha_{jet}} \right]^2 \right]^{1/2} \quad for \quad \alpha_{jk} > \alpha_{eq} \qquad (4)$$

$$ACOLD = \left[\frac{1}{A_{tot}} \sum_{jk} A_{jk} \left[\frac{\alpha_{jk} - \alpha_{eq}}{\alpha_{main} - \alpha_{jet}} \right]^2 \right]^{1/2} \quad for \quad \alpha_{jk} < \alpha_{eq} \qquad (5)$$

b) Mass flow weighted planar deviation parameters (also evaluated at x/R=1) as defined in Eq-6 through Eq-8 were also used to evaluate the mixing region. The MMIX value also equals the square root of the sum of the squared values of both MHOT and MCOLD. Note that these parameters are essentially the same as the area weighted parameters with the added density and velocity weighting terms.

$$MMIX = \left[\frac{1}{\dot{m}_{tot}} \sum_{jk} A_{jk} \rho_{jk} u_{jk} \left[\frac{\alpha_{jk} - \alpha_{eq}}{\alpha_{main} - \alpha_{jet}} \right]^2 \right]^{1/2} \qquad (6)$$

$$MHOT = \left[\frac{1}{\dot{m}_{tot}} \sum_{jk} A_{jk} \rho_{jk} u_{jk} \left[\frac{\alpha_{jk} - \alpha_{eq}}{\alpha_{main} - \alpha_{jet}} \right]^2 \right]^{1/2} \quad for \; \alpha_{jk} > \alpha_{eq} \qquad (7)$$

$$MCOLD = \left[\frac{1}{\dot{m}_{tot}} \sum_{jk} A_{jk} \rho_{jk} u_{jk} \left[\frac{\alpha_{jk} - \alpha_{eq}}{\alpha_{main} - \alpha_{jet}} \right]^2 \right]^{1/2} \quad for \; \alpha_{jk} < \alpha_{eq} \qquad (8)$$

c) The flow field was also evaluated by performing a numerical volume integration throughout the mixing section of interest. The volume integration parameters allow the quantification of the entire flow field mixture which is more descriptive of the overall flow phenomena in the mixing section as compared to a planar deviation analysis as performed with the mass flow weighted and area weighted parameters. This volume integration was performed on the temperature or equivalence ratio distributions depending if the configuration analyzed was either non-reacting or reacting respectively. The entire range of the normalized parameter f (from 0 to 1) was sub-divided into 200 equal size bins and the volume of the computational control volumes corresponding to the value of (f) at a certain bin size (f_i to $f_i + \Delta f$) was integrated. The integrated volume in each bin was normalized based on the entire analyzed mixer volume, thus obtaining the normalized volume fraction. The volume fraction for each bin was plotted in the ordinate with the corresponding value of f in the abscissa forming a histogram plot. In addition, the incremental partial volume per bin was integrated from f =0 to 1 and the cumulative volume fraction was obtained for all the 8 analyzed configurations. The cumulative volume fraction is also plotted versus (f) for all configurations. Note that the cumulative volume fraction

shown in this paper is the integrated histogram for (0≤f≤1). Therefore this value is generally independent of the bin size used in this analysis. Although not compared in this paper, the cumulative volume fraction for the interval $f_{equil} \pm \Delta f$ may be used to quantify the mixing uniformity within the tolerance Δf. In this paper however, the cumulative volume fraction is only used to indicate whether the histograms indeed integrate to a value of 1, as expected. The shape of the volume fraction histogram was also characterized by the definition of B(+) and B(-) similar to that used by (Oechsle, Mongia, and Holdeman, 1992). The value of B(+) is the "area determined" distribution half width above f_{equil} such that the integrated area under the histogram above f_{equil} is 1/2 that of the overall histogram area above f_{equil}. The same applies to B(-) for the area below f_{equil}. The definitions of B(+) and B(-) are shown pictorially in Figure-4. The best mixing results yield B(+) = B(-) = 0, meaning that the histogram distribution width effectively collapses towards the equilibrium value of (f) due to a homogeneous mixture of either temperature or equivalence ratio.

The results in this paper are presented in the following manner:

a) effect of reaction on mixing
b) effect of number of orifices/row on mixing, and
c) effect rich-zone equivalence ratio on mixing

Effect of reaction on mixing

The normalized temperature distribution results for all configurations for the axial-radial plane sections through the center of the jet are shown in Figure-5. The corresponding radial-tangential planes at x/R=1 are shown in Figure-6. Significant differences are apparent in the temperature distribution for the same configuration with similar operating conditions for both reacting and non-reacting cases. Note that the approach flow normalized temperature in the reacting flow cases is not the maximum value in the mixing section since the latter depends on the rich-zone equivalence ratio and is therefore not a conserved scalar. A lower approach mainstream normalized temperature value is expected with higher rich-zone equivalence ratio. These major differences are attributed to the fact that the reacting flow configurations are not only mixing hot and cold jets but also chemically reacting in areas permissible by the chemical kinetics of the species exiting the rich-zone of the combustor. It is worth noting that significant reaction occurs behind the orifice where the jet wake produces a low velocity recirculation between hot rich mixture exiting the rich-zone and relatively cold jets. This observation is shown for configuration # 2 and 4 (Figure-5b, 5d, 6b, and 6d) especially since both configurations have only 8 orifices. The configurations # 6 and 8 (Figure-5f, 5h, 6f, and 6h) however have 12 holes/row thus producing a much smaller jet trailing wake and therefore significantly inhibiting this reaction in the

mixing section. Note that the jet penetration for 8 orifices is greater than for 12 orifices and this is discussed later in more detail. The non-reacting flow fields are similar to the results reported by Oechsle, Mongia, and Holdeman 1992, and 1993. Note that in Figures-5 and 6, f=1 applies to the approach mainstream normalized temperature in the non-reacting flow configurations. Similarly, the stoichiometric temperature in the reacting flow configurations has a value of 1.

The normalized temperature distribution (f) in the non-reacting flows compare well with the normalized equivalence ratio distribution for all the configurations in Figures-7 and 8. These results seem to indicate that non-reacting temperature profiles can emulate the reacting flow mass flow distribution reasonably well. It is worth noting that the non-reacting jets appear to interact more at the center of the mixer at about x/R=0.5 as compared to the reacting flow jets, see (Figure-7a, 7b). This interaction is usually spotted by the upstream swirling flow produced at the location where opposing jets merge thereby inducing extra mixing between the mainstream and jet. This was not observed for the 12 orifice/row configurations due to shallow jet penetration produced by the 12 orifice/row configurations. Note that in Figure-7 and 8, f=0 represents the jet normalized temperature (non-reacting flow), and f=1 represents the mainstream normalized temperature (non-reacting flow).

The planar statistical variances indicate very similar conclusions to the observed temperature and equivalence ratio distributions. The area weighted and mass flow weighted parameters in Table-3 indicate very similar mixing non-uniformities between reacting and non-reacting cases for the same J, MR and DR at x/R=1. These results are also shown graphically in Figure-9a and 9b. The results indicate that the non-reacting flow configurations mix better compared to the reacting flow counterparts. Both area weighted and mass flow weighted results indicate similar results as shown previously in Oechsle, Mongia, and Holdeman, 1993. The volume fraction histogram results for all the configurations are shown in Figures-9c, 10, and 11. The B(+) and B(-) half width parameters are also tabulated in Table-3 and both indicate somewhat similar conclusions to the area weighted and mass flow weighted parameters; however, the differences between the volume fraction histogram shapes for reacting vs. non-reacting flow configurations with similar geometry and operating conditions are plotted in Figure-12. The results shown in Figure-12 indicate that for all comparable configurations the cumulative difference of the volume fraction/bin amounts from 50% to about 70% of the overall mixer volume of interest see Figure-12a, 12d. This observation is of significant value since particular mixing flow configurations may compare well at x/R=1 using both visually and planar average methodologies at x/R=1 but may be significantly different throughout the mixing section as shown by the volume integral results. This observation may have a significant effect on the future use of non-reacting flow configuration analysis when selecting a good mixing configuration for low NO$_x$ application.

The penetration of the jet for both reacting and non-reacting configurations are tabulated in Table-2 and the results are shown in Figure-13. The results indicate very little difference in both the penetration of the jet core and the jet width at x/R of 0.625, 1, and 2. It is important to note that although the change in the jet width is small according to the results shown in Table-2, the temperature and equivalence ratio cores of the jet as shown in Figure-6 and 8 for the reacting cases are significantly different compared to the non-reacting cores (noting that J, MR, and DR in the comparison are constant). Both temperature and equivalence ratio cores of the jet are significantly preserved throughout the flowfield up to x/R=1 for the reacting flow calculations only.

Effect of the number of orifices/row on mixing

The effect of the number of orifices/row on mixing has the expected results for constant J conditions. The results in Table-2 quantify the decrease in jet penetration with the increase in the number of jets as shown in Figure-13. Note that the streamlines depicted in Figure-13 indicate almost full turning of the jet by x/R=1 and these results correlate well with the temperature and equivalence ratio distribution plots indicating minor developments in the mixing flow field beyond x/R=1. The temperature and equivalence ratio profiles however indicate that enhanced mixing is obtained with the increase in the number of orifices for a given value of J as reported previously by Oechsle, Mongia, and Holdeman. (1992). The results obtained with the area weighted, mass flow weighted, and histogram parameters B(+) and B(-) indicate this same conclusion. The difference in the histograms between 8 and 12 orifices/row at similar J, MR and DR conditions are shown in Figure-14. Note that the histograms differ significantly in regions near f$_{equil}$ (Figure-14c and 14d). The reacting flow configurations (Fig-14b and 14d) show slightly less difference in mixing between 8 and 12 holes/row (with cumulative Δvol values of about 50%) as compared to the non-reacting configurations (Fig-14a, and 14c with Δvol values in excess of 60%).

As the number of holes increases, the jet wake volume decreases and therefore prevents the hot mainstream gas from entering and occupying this volume and reacting with cold jet stream which is recirculated in this wake. Both reacting and non-reacting results appear to be sensitive to the size of this jet trailing wake region as mentioned previously in this paper. The best mixing configuration from the 8 cases reported in this paper is the configuration number 7 shown in Figures-7g, 8g, and 11c. Note that the optimum mixer for a nominal J=25 is 9 holes/row as calculated in Eq-9 (Holdeman, 1993), where n is the number of orifices and C=2.5.

$$n = \frac{\pi \sqrt{2J}}{C} \qquad (9)$$

Effect of the rich-zone equivalence ratio on mixing

The effect of the increase of the rich-zone equivalence ratio (ϕ_{RZ}) from 1.35 to 1.80 is shown in Figures-5b, 5d, 6b, and 6d (temperature profiles) and Figures-7b, 7d, 8b, and 8d (equivalence ratio profiles). Significant differences in the temperature flow field are noted with the increase in rich-zone equivalence ratio. With a ϕ_{RZ} =1.35, the flow entering the mixing section need only mix slightly with the jet air to allow stoichiometric f/a to increase the temperature due to the expected chemical kinetics. However, the ϕ_{RZ} =1.80 configurations require a longer time to allow mixing of the rich mixture entering the mixing section, and the residence time of the mixing section limits the amount of further reaction occurring in the mixer. Therefore the temperature profiles are different as compared to the ϕ_{RZ} =1.35 configurations. This effect can be somewhat beneficial in the design of an RQL combustor since the ϕ_{RZ} appears to limit the location of the reaction between the rich mainstream flow and dilution jet mixing, thus allowing the designer to delay the reaction process after adequate mixing has been obtained in the mixing section. The difference in the amount of reaction in the mixing section is clearly shown in Figure-5f and 5h for ϕ_{RZ} of 1.35 and 1.80 consecutively. In addition to the delayed reaction produced by increased in ϕ_{RZ}, the mixing flowfield is slightly enhanced (see the results of configurations 1 and 3, 2 and 4, 5 and 7, and 6 and 8). Note that the volume histograms cannot be compared for in this case since the f_{equil} is a function of the ϕ_{RZ}.

Conclusions

1) The parameter (f) based on the non-reacting temperature profiles does not compare with the reacting flow normalized temperature solutions due to the additional reaction occurring in the mixing zone. The (f) parameter based on temperature and equivalence ratio however shows similar flow field solutions for non-reacting and reacting flows (respectively) since both are conserved scalar quantities.

2) The jet interaction between opposing jets becomes more significant for non-reacting flows calculations as compared to reacting flow results however, jet penetration itself appears not to have been significantly affected. The core of the jet appears to diffuse less and has less overall mixing in the reacting flow solutions as compared to the non-reacting cases.

3) All three statistical parameters, area weighted, mass flow weighted, and histogram half widths correlate well for the selection of the best mixing configuration (configuration #7). Significant differences are shown in the histogram shapes between reacting and non-reacting flows that are not shown using simple planar statistical parameters. This indicates that additional study is necessary to evaluate the use of planar averages in characterizing the mixing flow phenomena, and in particular, extrapolating the expected NO_x formation in a

mixing section of an RQL combustor based on results valued at x/R=1.

4) Increase in the number of orifices decreases the overall volume of the wake behind each jet and therefore significantly affects the reaction in this area. The wake region behind the jet is an optimum location for flame stability due to low velocity recirculation areas where mainstream rich fuel mixture is mixed with relatively cold jet air to enhance reaction.

5) An increase in rich-zone equivalence ratio (ϕ_{RZ}) produces an effective reaction delay in the mixing section; therefore, the selection of the appropriate ϕ_{RZ} allows the combustor designer to delay this mixing zone reaction sufficiently to allow adequate mixing to occur.

References

Bain, D.B., Smith, C.E., and Holdeman, J.D.,"CFD Mixing Analysis of Jets Injected from Straight and Slanted Slots into Confined Crossflow in Rectangular Ducts," AIAA paper No. 92-3087 (1992). (Also NASA TM 105699).

Bain, D.B., Smith, C.E., and Holdeman, J.D.,"Parametric CFD Analysis of Jet Mixing into Confined Crossflow in Rectangular Ducts," AIAA paper No. 93-2044 (1993). (Also NASA TM 106179).

Bruce, T.W., Mongia, H.C., and Reynolds, R.S., "Combustion design criteria validation," (1979), (USARTL-TR-78-55A, B, and C).

Doerr, Th., and Hennecke, D.K., " The Mixing Process in the Quenching Zone of the Rich-Lean-Combustion Concept," AGARD-PEP 81st Sympossium of Fuels and Combustion Technology for Advanced Aircraft Engines, (1993).

Hatch, M.S., Sowa, W.A., Samuelsen, G.S., and Holdeman, J.D., "Jet Mixing Into a Heated Cross Flow in a Cylindrical Duct: Influence of Geometry and Flow Variations," AIAA Paper No. 92-0773 (1992). (Also NASA TM 105390).

Holdeman, J.D., "Mixing of Multiple Jets with a Confined Subsonic Crossflow," Prog. Energy Combust. Sci., (1993), Vol 19, pp 31-70. (Also see AIAA Paper No. 91-2458 (1991), and NASA TM 104412).

Howe, G.W., Li, Z., Shih, T.I.-P., and Nguyen, H.L.,"Simulation of mixing in the quick quench region of a rich burn -

quick quench mix - lean burn combustor." AIAA Paper No. 91-0410 (191).

Kroll, J.T., Sowa, W.A., Samuelsen, G.S., and Holdeman, J.D.,"Optimization of Circular Orifice Jets Mixing into a Heated Crossflow in a Cylindrical Duct." AIAA Paper No. 93-0249 (1993).

Launder, B.E., and Spalding, D.B.," Lectures in Mathematical Models of Turbulence," Academic Press Inc. (London) LTD., (1972).

Liscinsky, D.S., True, B., Vranos, A., and Holdeman, J.D., "Experimental Study of Cross-Stream Mixing in a Rectangular Ducts." AIAA Paper No. 92-3090 (1992). (Also NASA TM 106194).

Liscinsky, D.S., True, B., and Holdeman, J.D., "Experimental Investigation of Crossflow Jet Mixing in a Rectangular Duct." AIAA Paper No. 93-2037 (1993). (Also NASA TM 106152).

Oechsle, V.L., Mongia, H.C., and Holdeman, J.D. " A Parametric Numerical Study of Mixing in a Cylindrical Duct." AIAA Paper No. 92-3088 (1992). (Also NASA TM 105695).

Oechsle, V.L., Mongia, H.C., and Holdeman, J.D. " An Analytical Study of Jet Mixing in a Cylindrical Duct." AIAA Paper No. 93-2043 (1993). (Also NASA TM 106181).

Patankar.S.V., " Numerical Heat Transfer and Fluid Flows," Hemisphere, Washington D.C. (1980).

Rizk, N.K., Mongia, H.C., "Ultra-Low NO_x Rich Lean Combustion." ASME Paper No. 90-GT-87 (1990).

Rizk, N.K., Mongia, H.C., "Low NO_x Rich-Lean Combustion Concept Application." AIAA Paper No. 91-1962 (1991).

Rizk, N.K., Mongia, H.C., "Three-Dimensional NO_x Model for Rich/Lean Combustor." AIAA Paper No. 93-0251 (1993).

Shaw, R.J., "Engine Technology Challenges for a 21st Century High Civil Speed Transport." AIAA 10th International Symposium on Air Breathing Engines (1991). (Also NASA TM 104361).

Smith, C.E., Talpallikar, M.V., and Holdeman, J.D.,"A CFD Study of Jet Mixing in Reduced Flow Areas for Lower Combustion Emissions." AIAA Paper No. 91-2460 (1991). (Also NASA TM 104411).

Talpallikar, M.V., Smith, C.E., Lai, M.C., and Holdeman, J.D., " CFD Analysis of Jet Mixing in Low NO_x Flametube Combustors." J. Eng. Gas Turbine Pwr. 114, 416 (1992). (Also ASME Paper No. 91-GT-217; NASA TM 104466).

Vranos, A., Liscinsky, D.S., True, B., and Holdeman, J.D.," Experimental Study of Cross-Stream Mixing in a Cylindrical Duct." AIAA Paper No. 91-2459 (1991). (Also NASA TM 105180).

Zhu, G., and Lai, M.-C., "A parametric study of penetration and mixing of radial jets in necked-down cylindrical cross-flow," AIAA Paper No. 92-3091 (1992).

CASE	Units	1	2	3	4	5	6	7	8
OVERALL									
J (jet/main)		25.0	25.0	25.0	25.0	25.0	25.0	25.0	25.0
MR (jet.main)		1.83	1.83	2.67	2.67	1.83	1.83	2.67	2.67
DR (jet/main)		2.578	2.584	2.300	2.231	2.578	2.584	2.300	2.231
VR (jet/main)		3.114	3.110	3.297	3.347	3.114	3.110	3.297	3.347
Ar (jet/main)		0.228	0.228	0.352	0.358	0.228	0.228	0.352	0.358
Phi (rich zone)		0.00	1.35	0.00	1.80	0.00	1.35	0.00	1.80
Phi (lean zone)		0.00	0.45	0.00	0.45	0.00	0.45	0.00	0.45
DP/P	%	2.91	3.08	3.00	3.10	3.00	3.00	3.00	3.10
MAINSTREAM									
P main	atm.	1.0	13.4	1.0	13.4	1.0	13.4	1.0	13.4
T main	K	773	2,527	690	2,182	773	2,527	690	2,182
V main	m/sec	22.7	42.3	21.8	39.4	23.1	41.7	21.8	39.4
M main	kg/sec	0.052	0.399	0.056	0.431	0.045	0.393	0.056	0.430
Mixer Diameter	m	0.080	0.080	0.080	0.080	0.080	0.080	0.080	0.080
JET		Circular	Circular	Circular	Circular	Circular	Circular	Circular	Circular
P jet	atm.	1.0	13.4	1.0	13.4	1.0	13.4	1.0	13.4
T jet	K	300	978	300	978	300	978	300	978
V jet	m/sec	70.8	131.7	71.9	131.9	71.9	129.8	71.9	131.9
M jet	kg/sec	0.096	0.731	0.150	1.150	0.083	0.720	0.150	1.149
ACd jet/row	m²	1.15e-03	1.14e-03	1.77e-03	1.80e-03	1.15e-03	1.14e-03	1.77e-03	1.80e-03
Orifice Cd		0.80	0.81	0.80	0.82	0.80	0.80	0.80	0.82
Number of orifices		8	8	8	8	12	12	12	12
Blockage		0.430	0.430	0.534	0.538	0.527	0.526	0.654	0.659
Orifice T.E. x/R		0.338	0.338	0.420	0.423	0.276	0.276	0.343	0.345
Flow Condition		NR	REACT	NR	REACT	NR	REACT	NR	REACT

Table-1. Overall description of the operating conditions and geometric configurations

Conf	Jet Penetration @ x/R =0.625		Jet Penetration @ x/R = 1.0		Jet Penetration @ x/R= 2.0	
	w/R	Penetration of jet core / R	w/R	Penetration of jet core / R	w/R	Penetration of jet core / R
1	0.425	0.7	0.35	0.75	0.325	0.75
2	0.4	0.675	0.35	0.725	0.325	0.725
3	0.475	0.625	0.45	0.675	0.375	0.7
4	0.475	0.575	0.425	0.625	0.35	0.675
5	0.325	0.575	0.325	0.625	0.3	0.65
6	0.35	0.575	0.325	0.625	0.3	0.65
7	0.425	0.55	0.4	0.6	0.375	0.6
8	0.425	0.5	0.425	0.55	0.375	0.575

Table-2. Jet penetration development through the center of the jet in the circumferential direction

Config	condition	# holes	PHI RZ	MR	AMIX	AHOT	ACOLD	MMIX	MHOT	MCOLD	B(-)	B(+)
1	NR	8	0	1.83	0.21	0.187	0.096	0.223	0.195	0.108	0.171	0.266
2	REACT	8	1.35	1.83	0.221	0.191	0.111	0.223	0.195	0.108	0.182	0.333
3	NR	8	0	2.67	0.173	0.154	0.079	0.184	0.162	0.085	0.148	0.255
4	REACT	8	1.8	2.67	0.201	0.175	0.1	0.209	0.178	0.109	0.179	0.328
5	NR	12	0	1.83	0.164	0.144	0.079	0.165	0.138	0.091	0.157	0.207
6	REACT	12	1.35	1.83	0.171	0.144	0.093	0.171	0.132	0.108	0.166	0.244
7	NR	12	0	2.67	0.144	0.13	0.062	0.139	0.118	0.074	0.136	0.169
8	REACT	12	1.8	2.67	0.166	0.142	0.082	0.164	0.131	0.098	0.159	0.288

Table-3. Summary of the mixing non-uniformity results for all the analyzed configurations

NOTE: REACT = Reacting flow , NR = Non-reacting flow, PHI RZ = rich-zone equivalence ratio
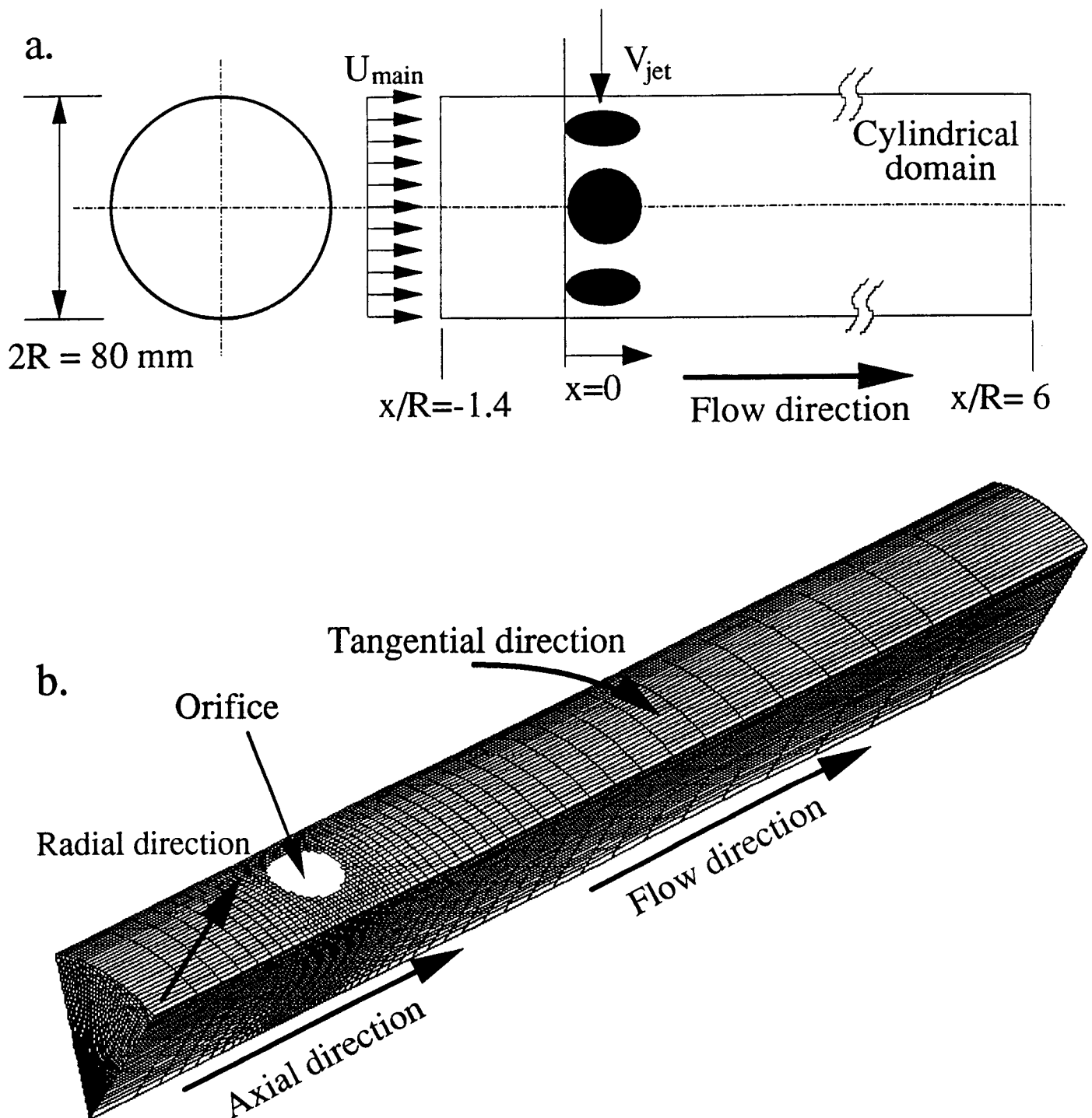
Figure 1. Depiction of (a.) geometric configuration of the mixing section and (b.) typical computational grid.

Configuration #

REACTING

NON-REACTING

8

12

NUMBER OF ORIFICES

$\phi = 1.80$
MR=2.67

$\phi = 1.35$
MR=1.83

RICH ZONE EQUIVALENCE RATIO AND
MASS FLOW RATIO VARIATION
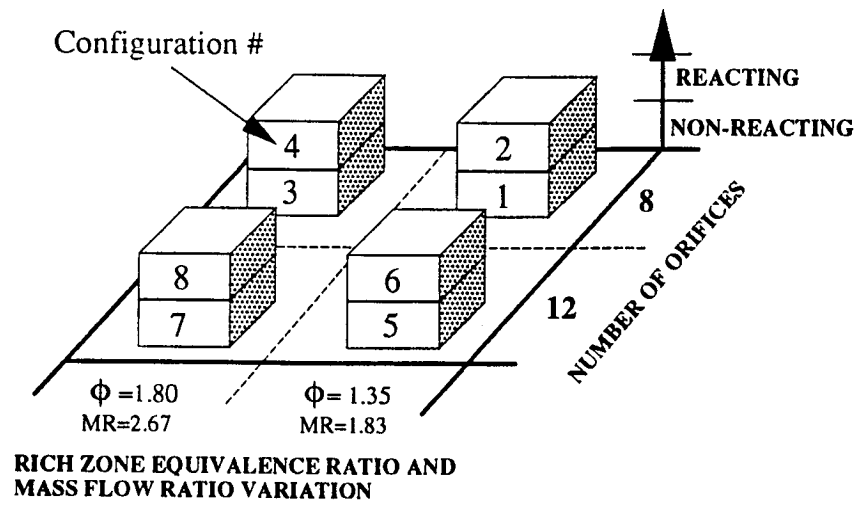
Figure-2. Matrix of analyzed configurations

Jet flow inlet

Penetration of
jet core

Jet width, W

Mainstream flow inlet

flow direction

x/R=0

x/R=1

Axial-radial plane through the center of the jet
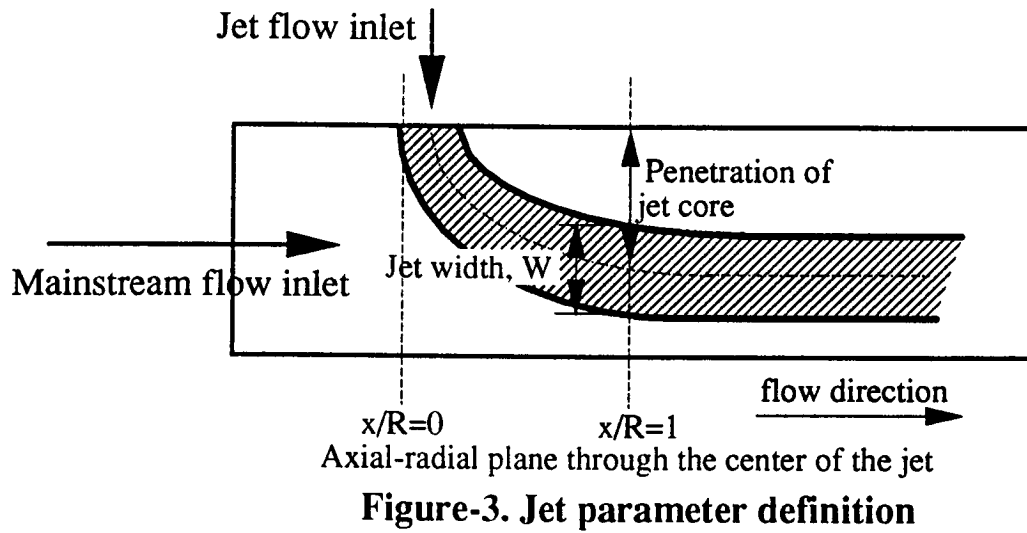
Figure-3. Jet parameter definition

1

B(-)

B(+)

Cumulative volume fraction

$(\delta+1)/2$

δ

$\delta/2$

Histogram

0

0

f_{equil}

f

1
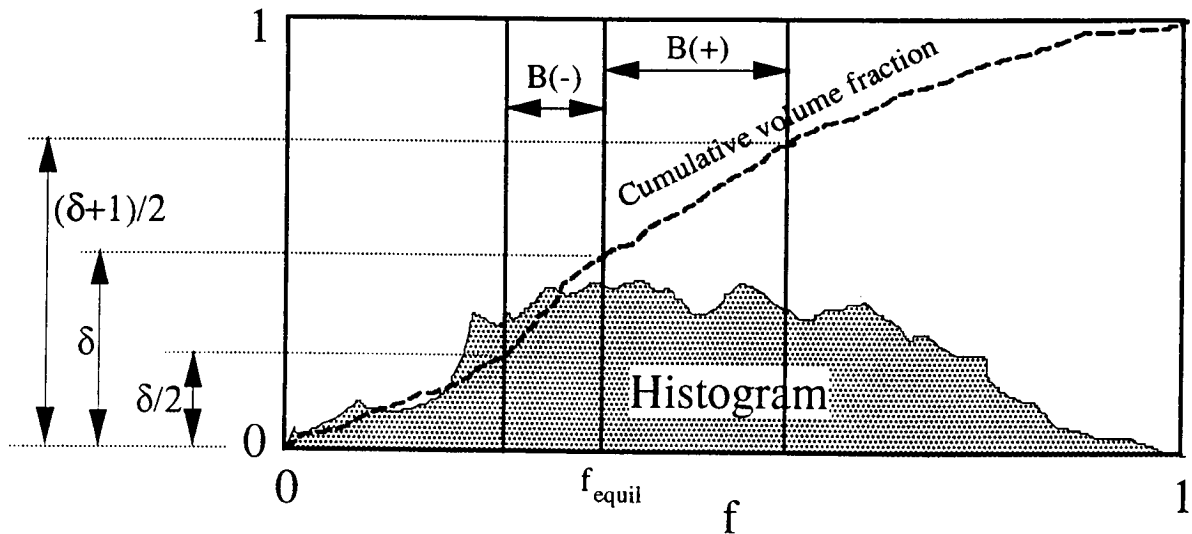
Figure-4. Graphical definition of B(+) and B(-)
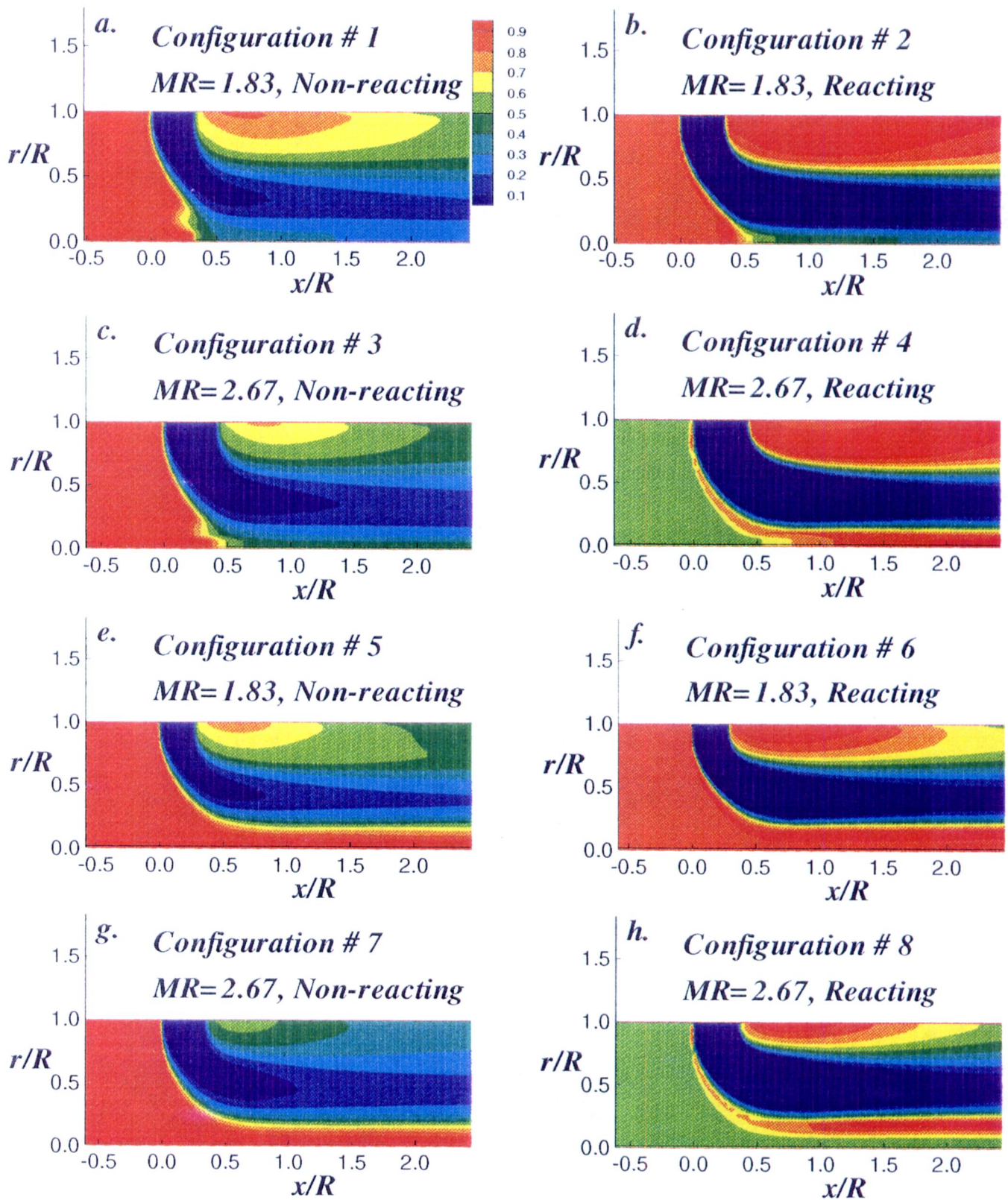
Figure-5. Normalized Temperature distribution through the center of the jet

(a., b., c., and d.) 8 round orifices / row

(e., f., g., and h.) 12 round orifices / row

jet = 0
mainstream = 1 (non-react flows)
stoichiometry = 1 (react flows)

13
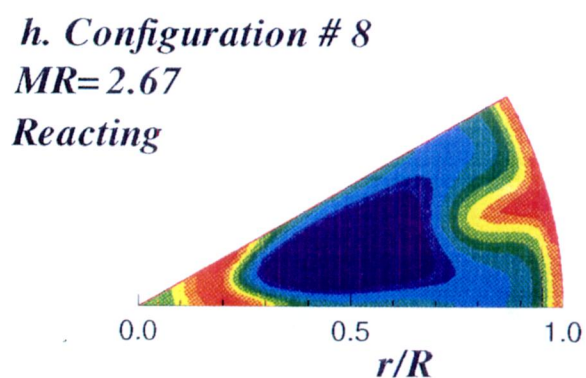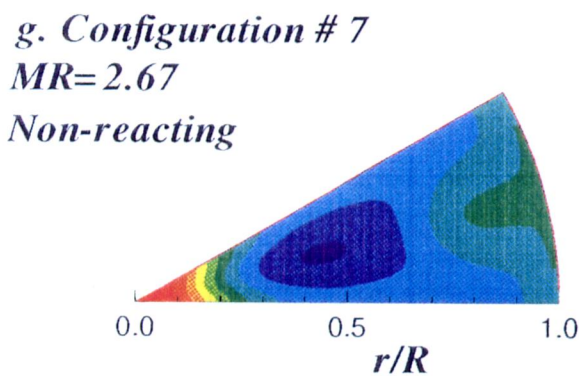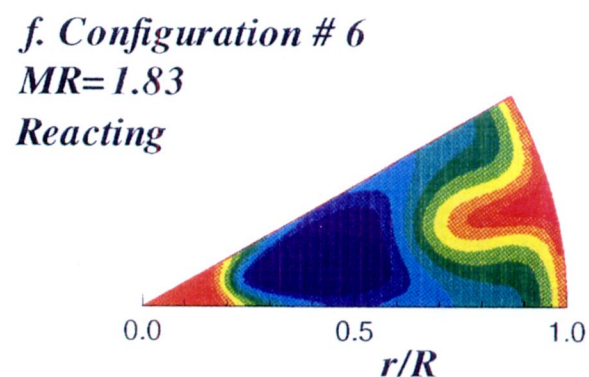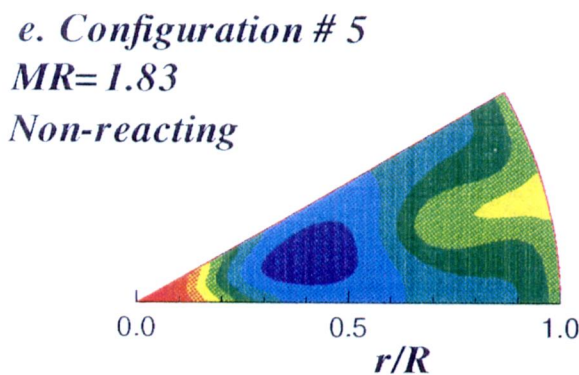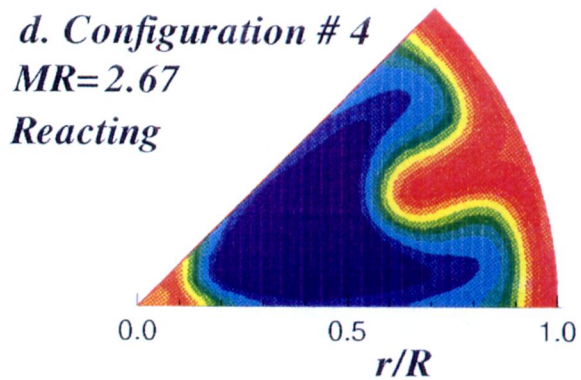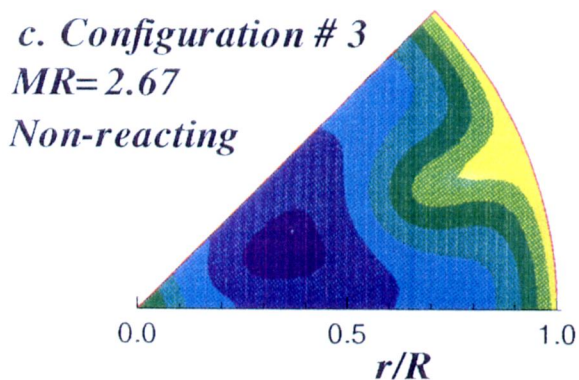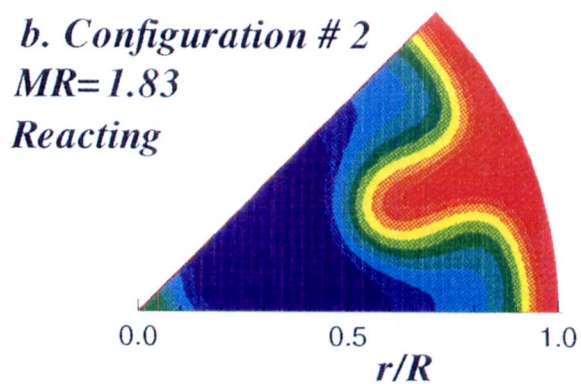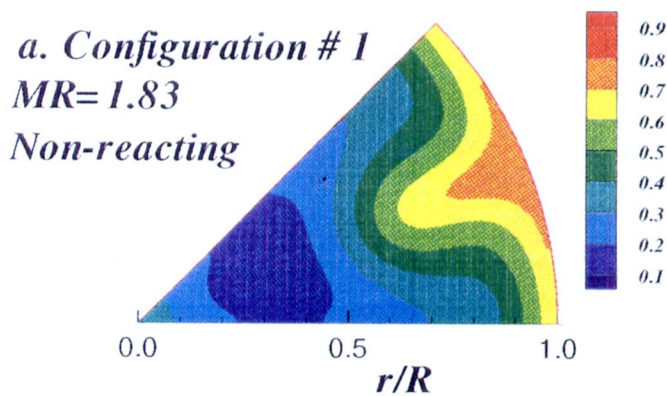
Figure-6. Normalized temperature distribution in the radial-tangential plane at x/R= 1

(a., b., c., and d.) 8 round orifices / row
(e., f., g., and h.) 12 round orifices / row

jet = 0
mainstream = 1 (non-reacting flows)
stoichiometry = 1 (reacting flows)
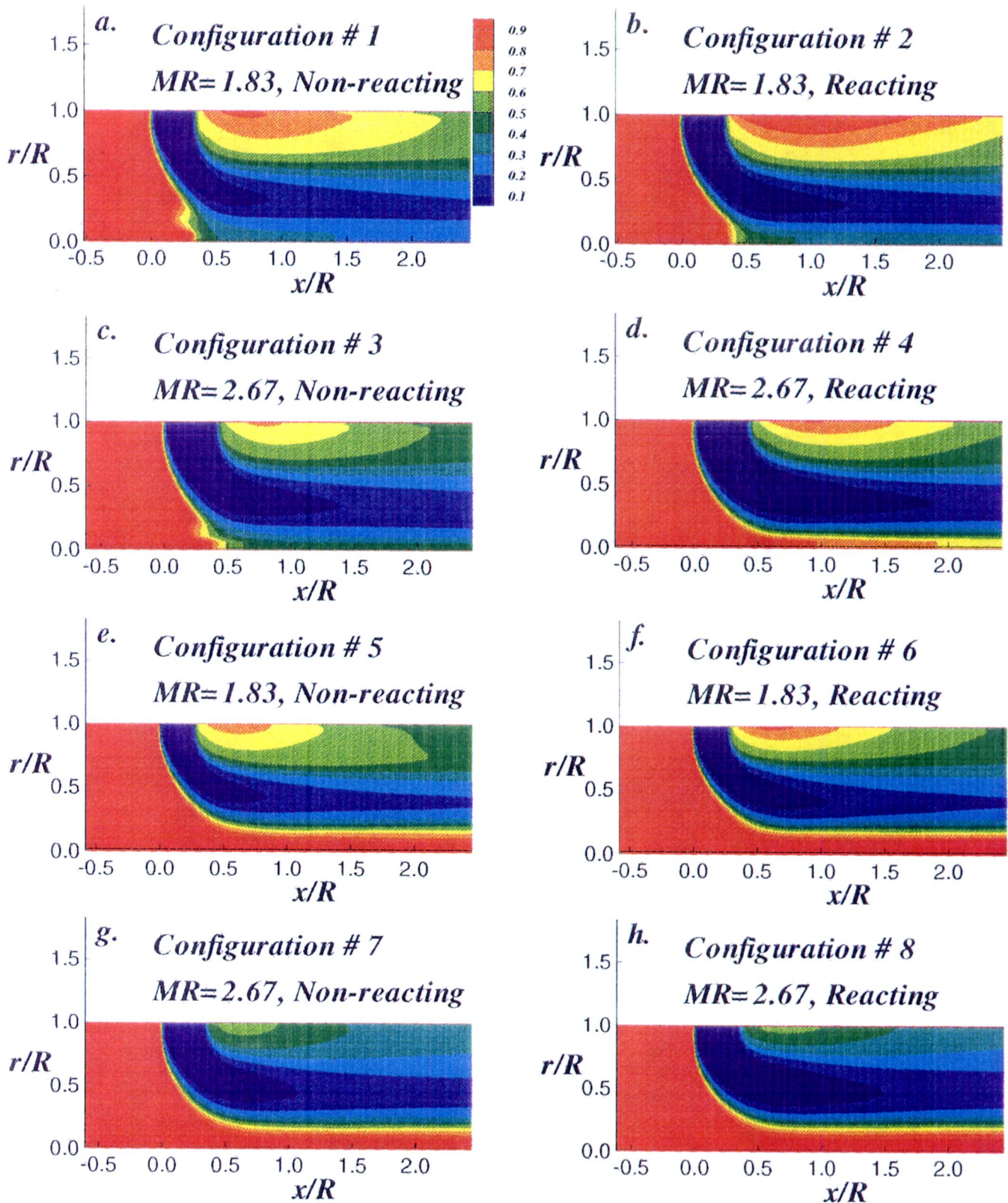
Figure-7. Normalized Temperature distribution (f) (non-reacting flow) compared to the normalized equivalence ratio distribution (f) (reacting flow)-- (plane through the center of the jet)

(a., b., c., and d.) 8 round orifices / row
(e., f., g., and h.) 12 round orifices / row

$f=0$ at T_{jet} or ϕ_{jet}
$f=1$ at T_{main} or ϕ_{main}
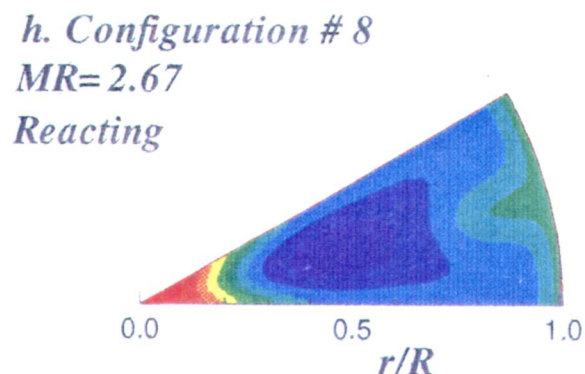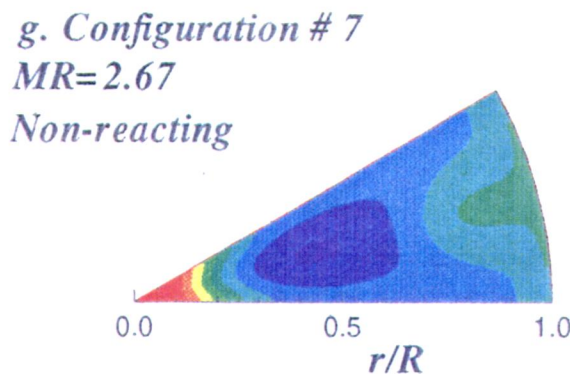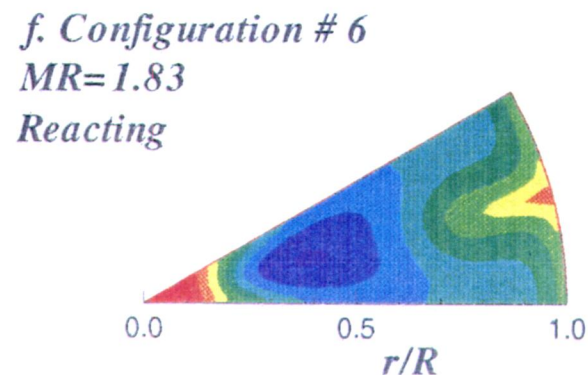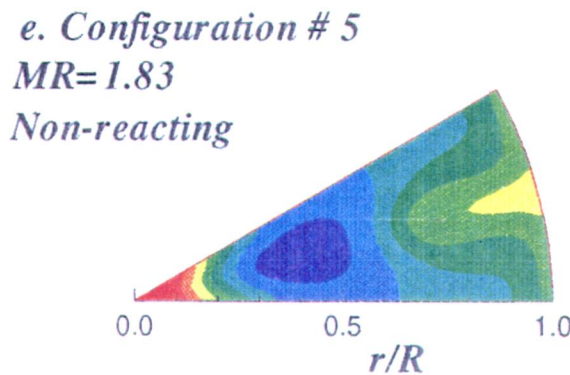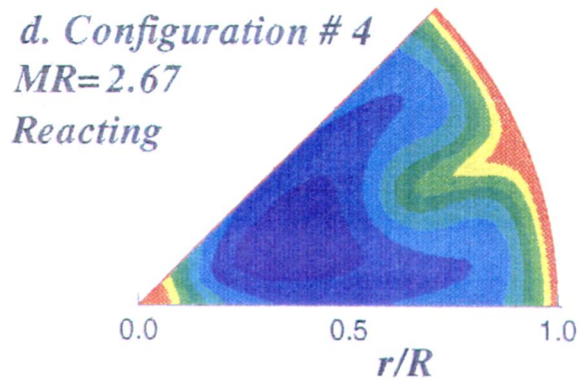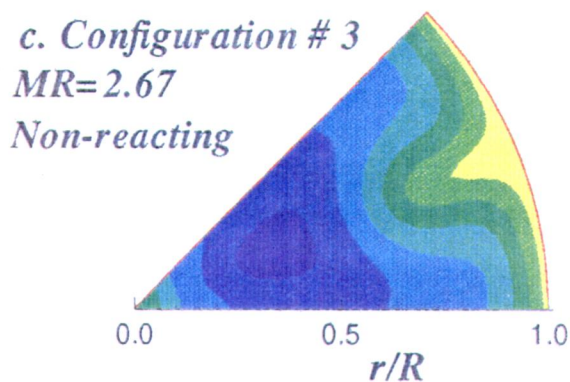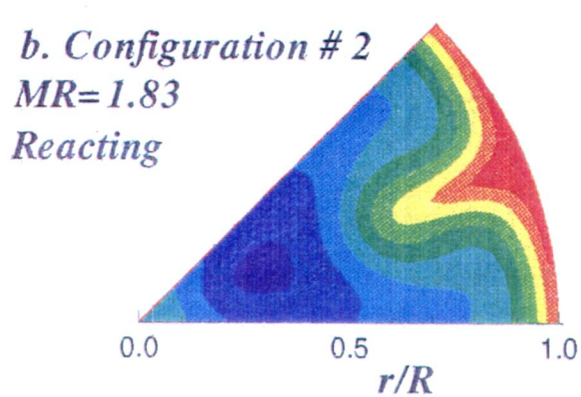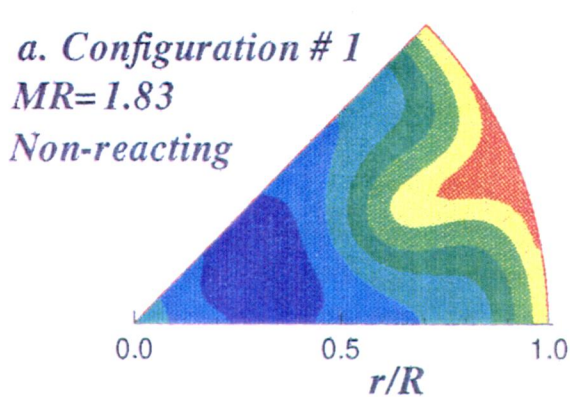
Figure-8. *Normalized temperature (f) for the non-reacting flow compared to the normalized equivalence ratio (f) for the reacting flow for radial-tangential plane at x/R=1*

(a., b., c., and d.) 8 round orifices / row
(e., f., g., and h.) 12 round orifices / row

$f=0$ at T_{jet} or ϕ_{jet}
$f=1$ at T_{main} or ϕ_{main}
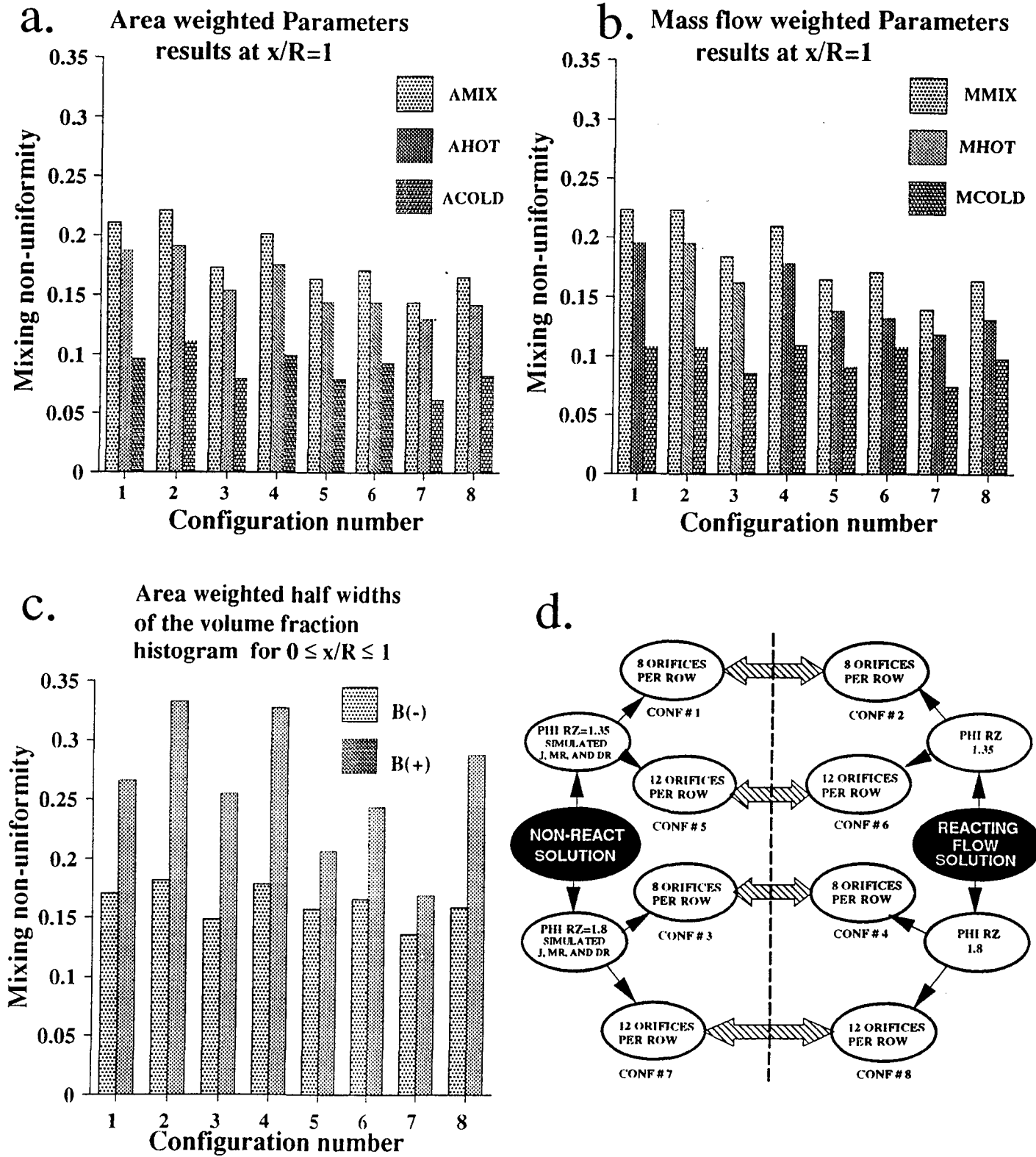
Figure-9. Mixing non-uniformity parameters (Table-3).
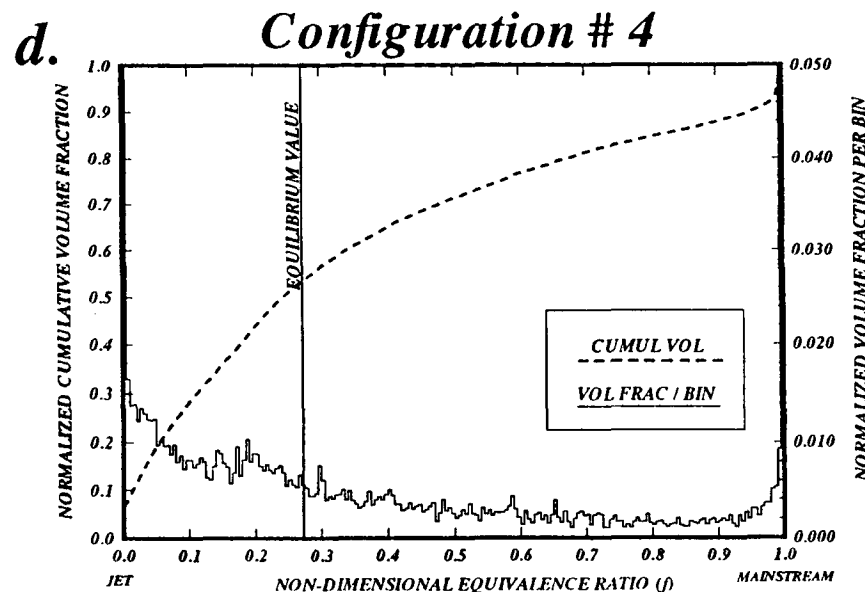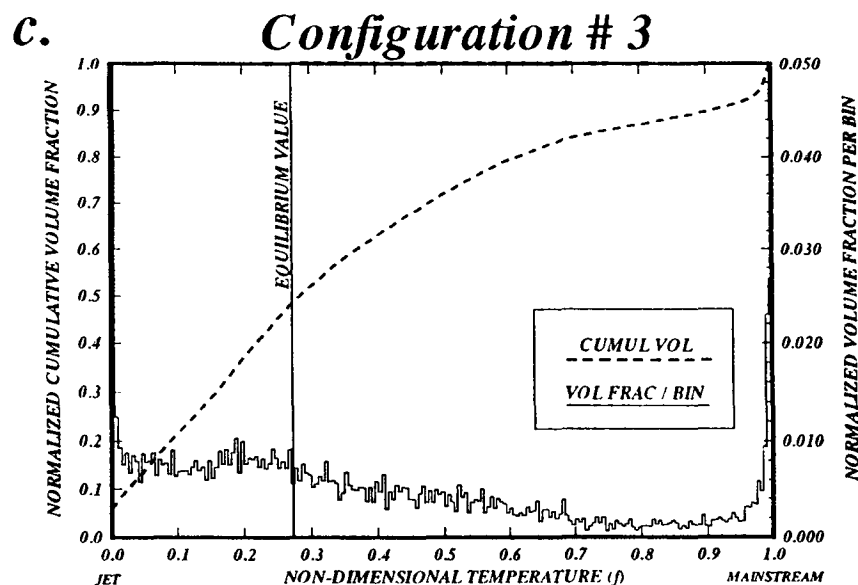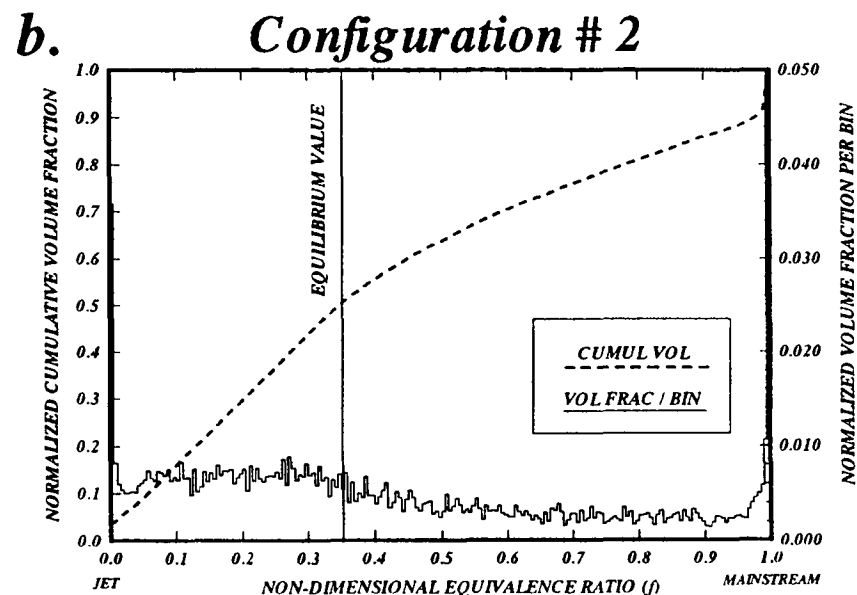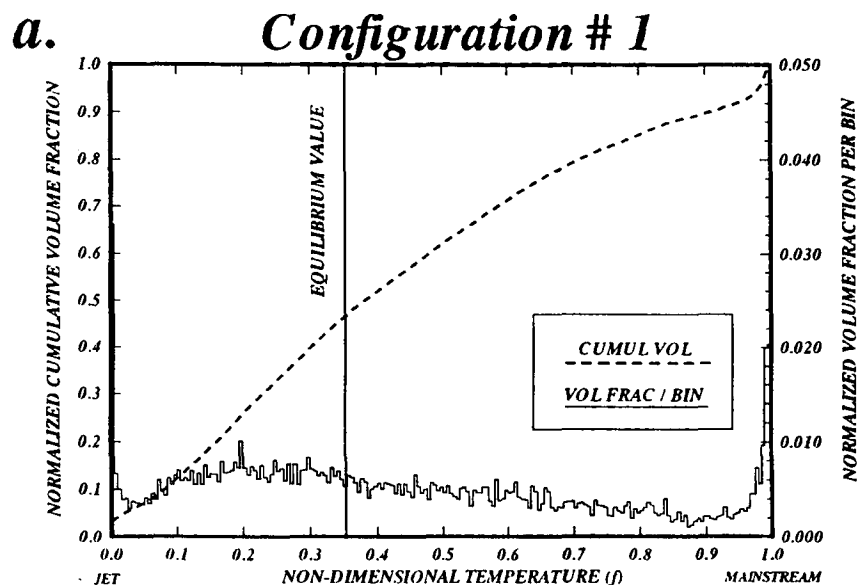
(a.) Conf # 1: MR=1.83, 8 holes/row, non-reacting   (b.) Conf # 2: MR=1.83, 8 holes/row, ϕ_{RZ} = 1.35, reacting

(c.) Conf # 3: MR=2.67, 8 holes/row, non-reacting   (d.) Conf # 4: MR=2.67, 8 holes/row, ϕ_{RZ} =1.80, reacting

Figure-10. Mixing non-uniformity volume integration parameters for a total of 200 bins (for 0 <= x/R <= 1)
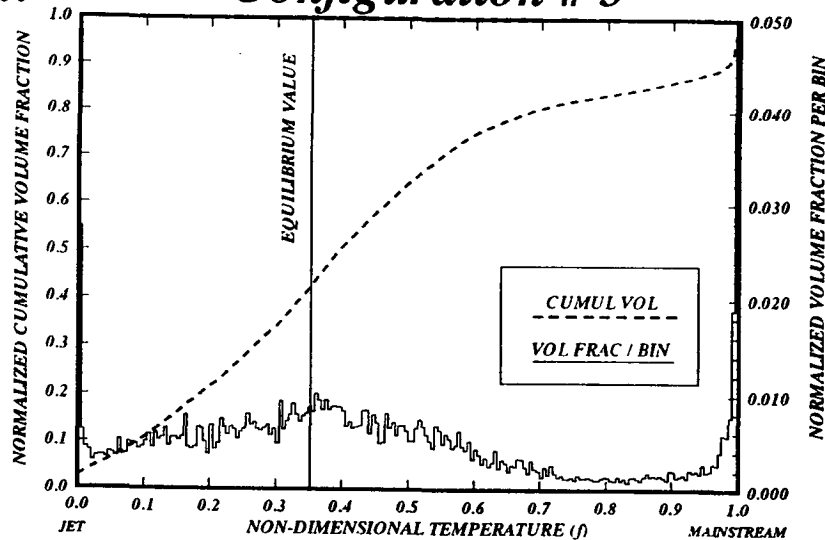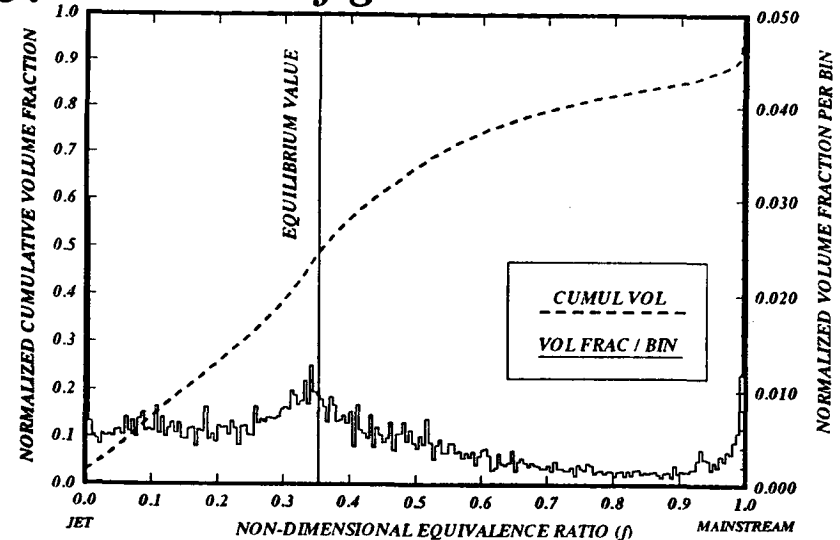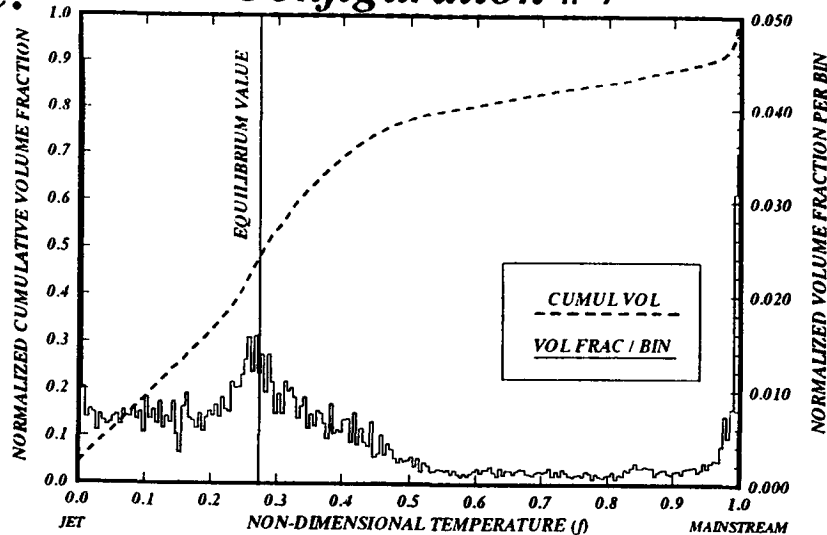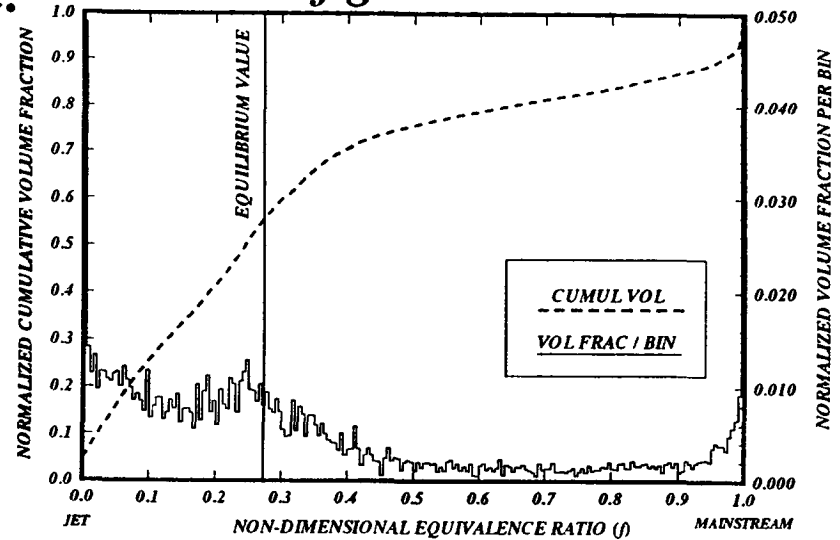
(a.) Conf # 5: MR=1.83, 12 holes/row, non-reacting

(b.) Conf # 6: MR=1.83, 12 holes/row, ϕ_{RZ} = 1.35, reacting

(c.) Conf # 7: MR=2.67, 12 holes/row, non-reacting

(d.) Conf # 8: MR=2.67, 12 holes/row, ϕ_{RZ} =1.80, reacting

Figure-11. Mixing non-uniformity volume integration parameters for a total of 200 bins for (0 <= x/R <= 1)

a. Δ *Fractions for Conf (1 - 2)*
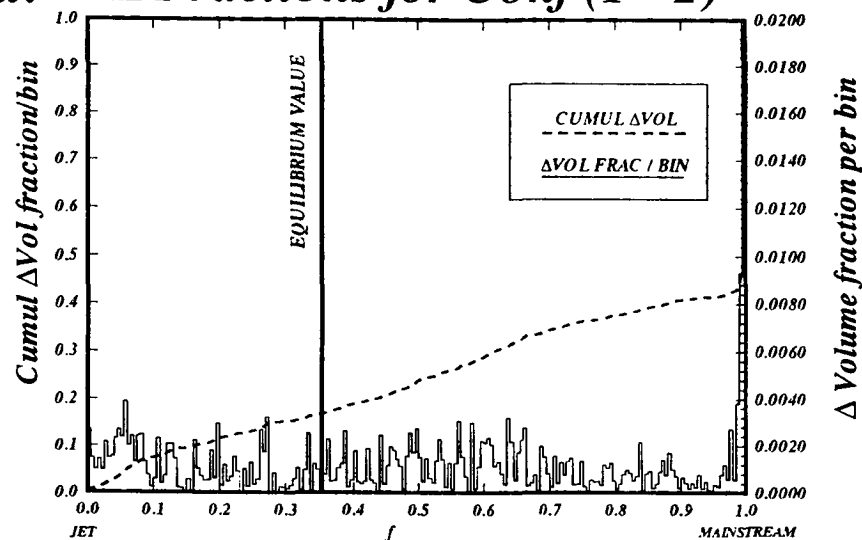
b. Δ *Fractions for Conf (3 - 4)*
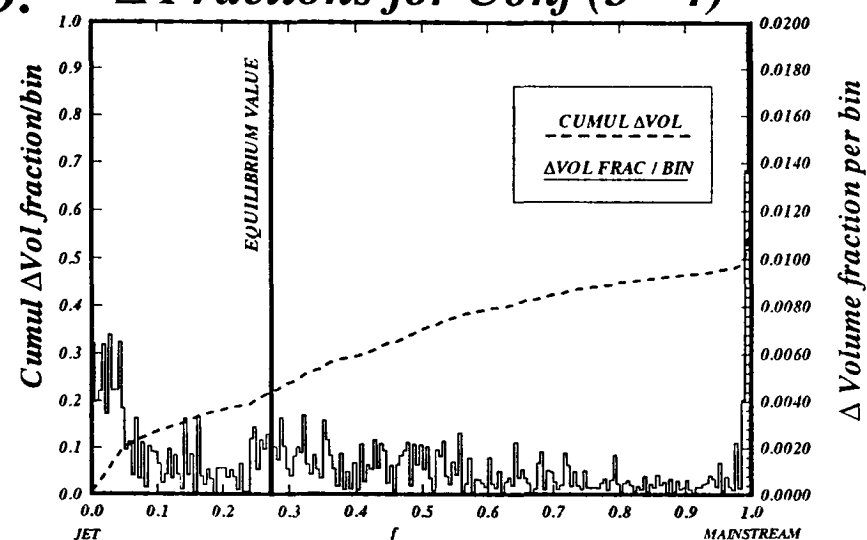
c. Δ *Fractions for Conf (5 - 6)*
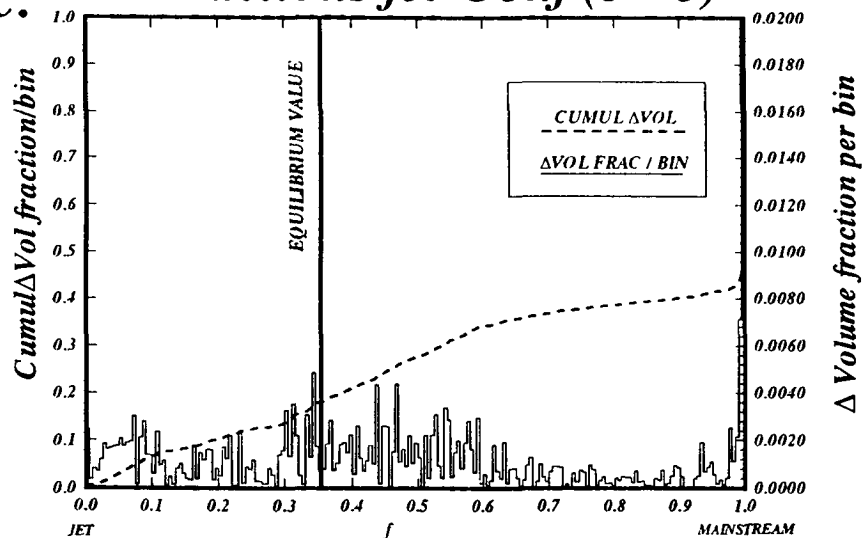
d. Δ *Fractions for Conf (7 - 8)*
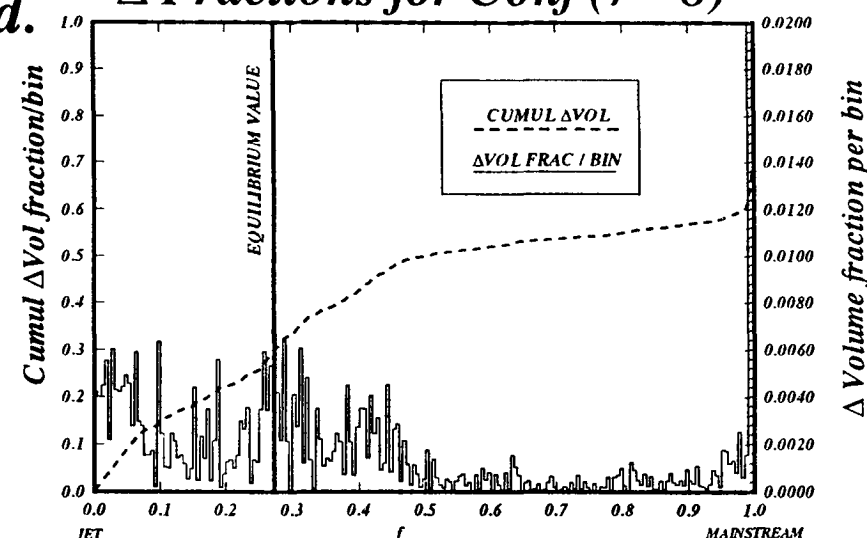
a. Δ(1 - 2), MR=1.83, 8 holes/row   *b.* Δ(3 - 4), MR=2.67, 8 holes/row

c. Δ(5 - 6), MR=1.83, 12 holes/row   *d.* Δ(7 - 8), MR=2.67, 12 holes/row

Figure-12. Difference between the reacting and non-react configurations for the same geometry and operating conditions
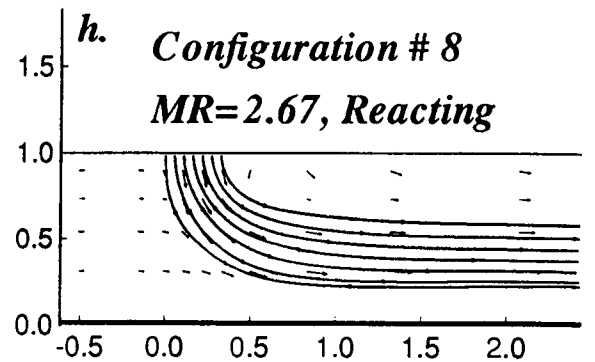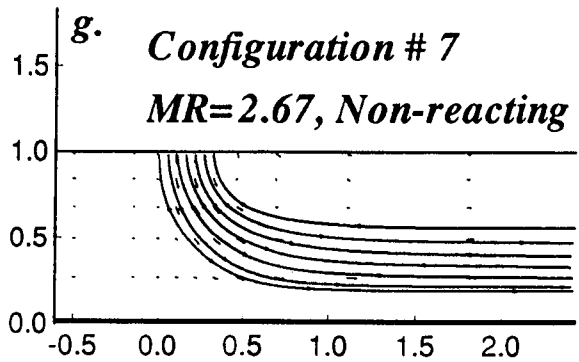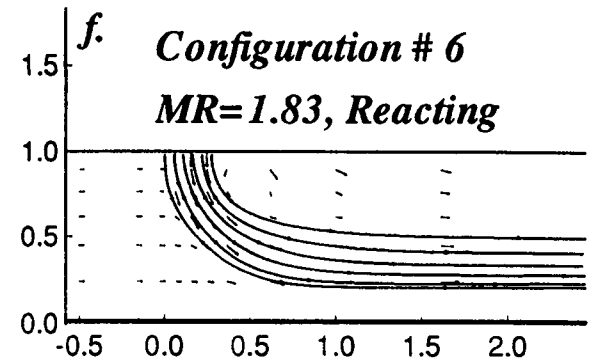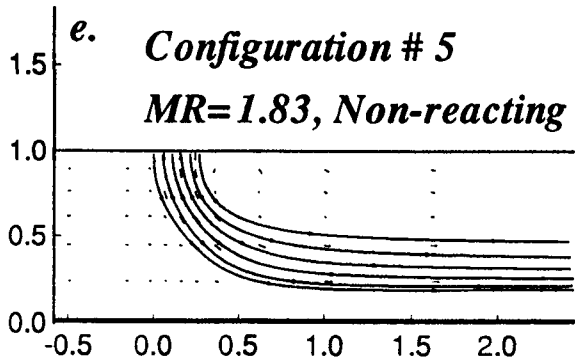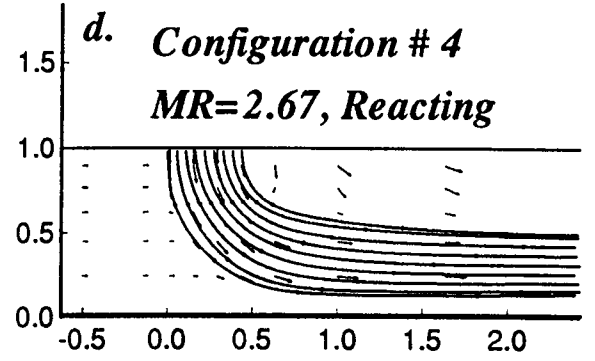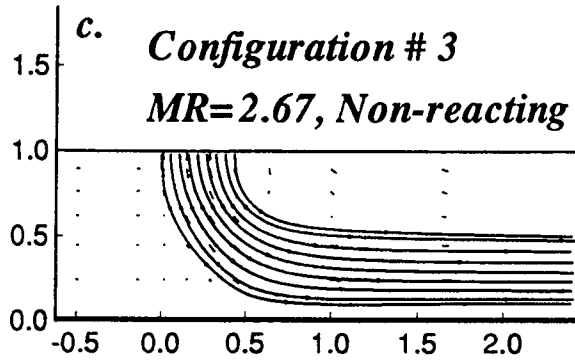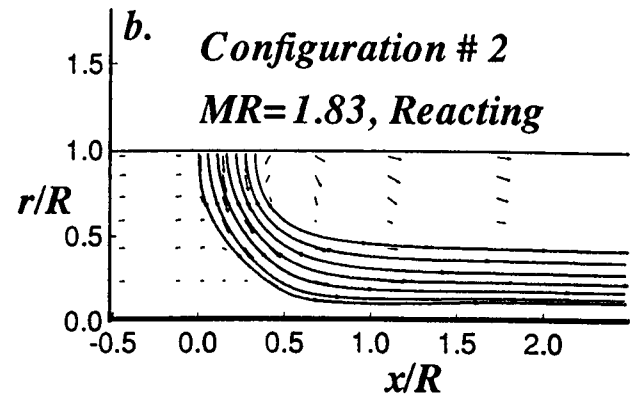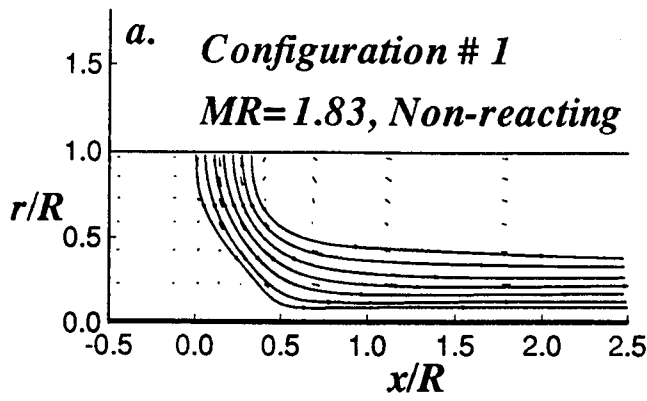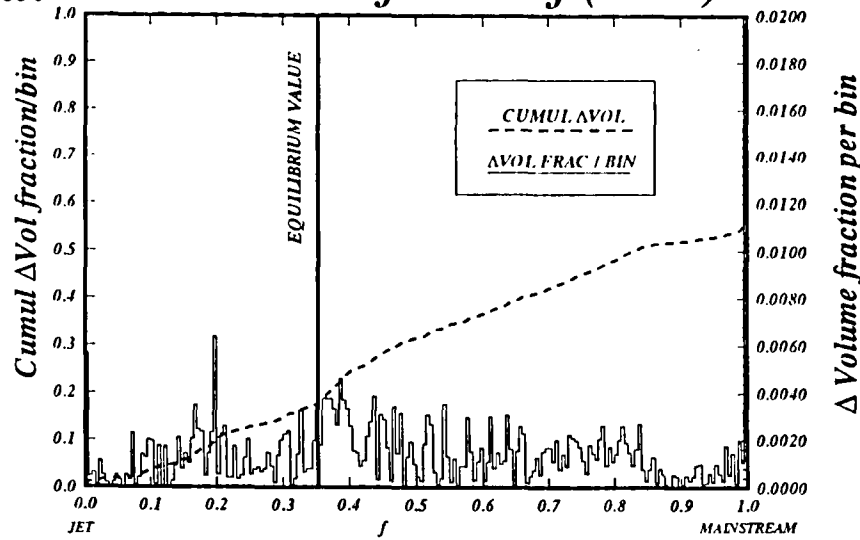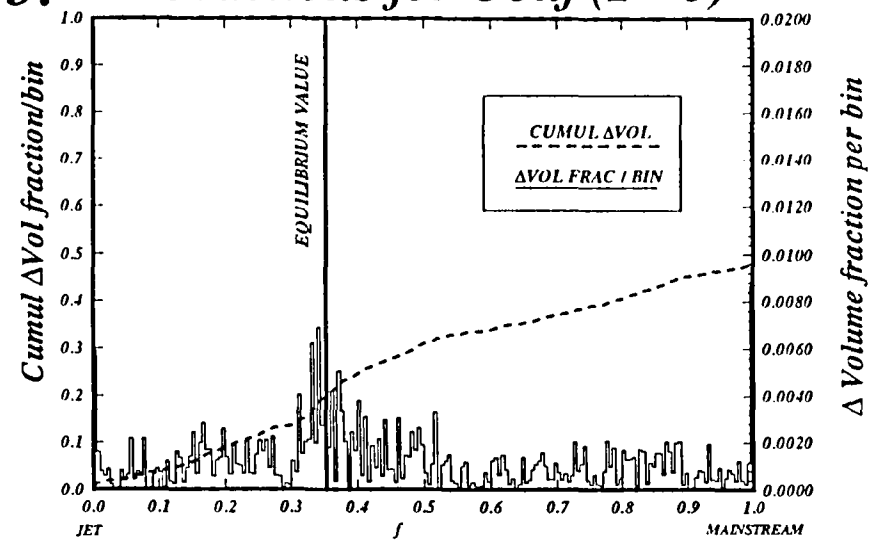
Figure-13. Jet penetration as seen through the center of the jet
(a., b., c., and d.) 8 round orifices / row
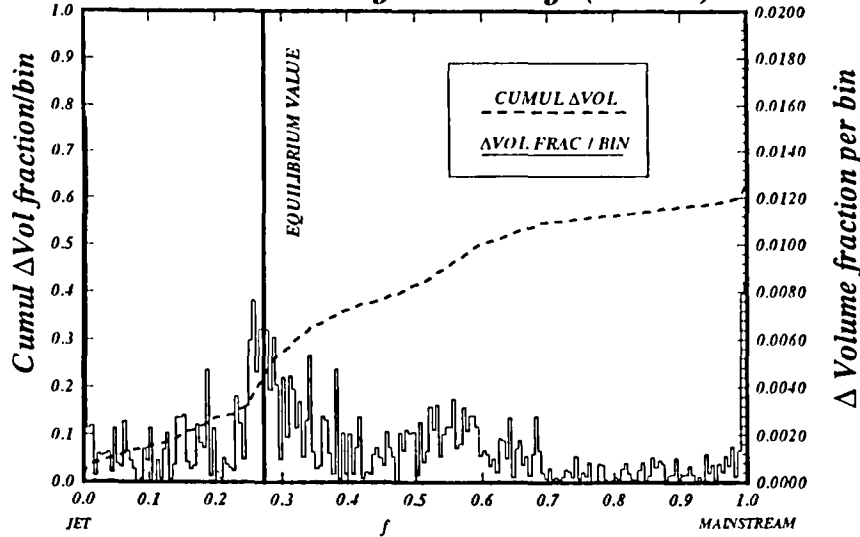*(e., f., g., and h.) 12 round orifices / row*

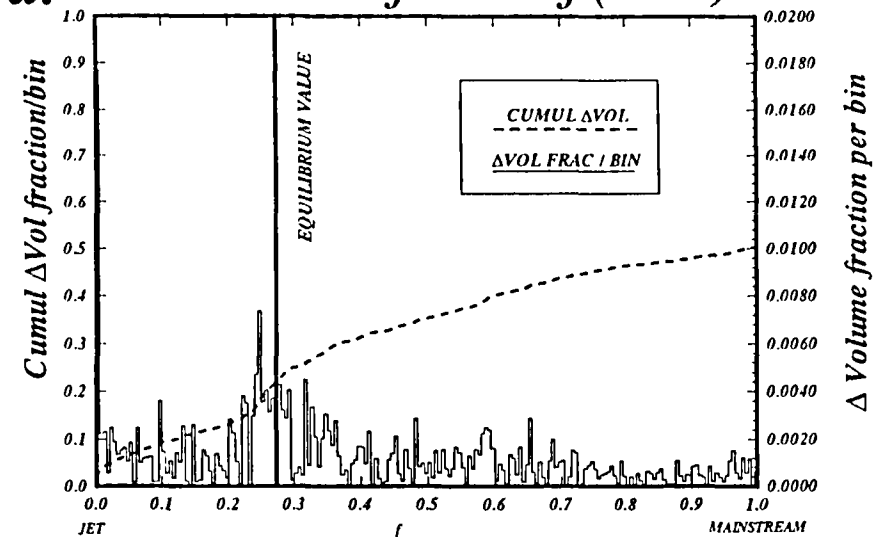a. Δ(1 - 5), MR=1.83, non-reacting   b. Δ(2 - 6), MR=1.83, reacting
c. Δ(3 - 7), MR=2.67, non-reacting   d. Δ(4 - 8), MR=2.67, reacting

Figure-14. Effect of the variation of the number of holes/row on mixing.

REPORT DOCUMENTATION PAGE

Public reporting burden for this collection of information is estimated to average 1 hour per response, including the time for reviewing instructions, searching existing data sources, gathering and maintaining the data needed, and completing and reviewing the collection of information. Send comments regarding this burden estimate or any other aspect of this collection of information, including suggestions for reducing this burden, to Washington Headquarters Services, Directorate for Information Operations and Reports, 1215 Jefferson Davis Highway, Suite 1204, Arlington, VA 22202-4302, and to the Office of Management and Budget, Paperwork Reduction Project (0704-0188), Washington, DC 20503.

1. AGENCY USE ONLY (Leave blank)	2. REPORT DATE	3. REPORT TYPE AND DATES COVERED
	January 1994	Technical Memorandum

4. TITLE AND SUBTITLE

Comparison of Mixing Calculations for Reacting and Non-reacting Flows in a Cylindrical Duct

5. FUNDING NUMBERS

WU–537–02–21

6. AUTHOR(S)

V.L. Oechsle, H.C. Mongia, and J.D. Holdeman

7. PERFORMING ORGANIZATION NAME(S) AND ADDRESS(ES)

National Aeronautics and Space Administration
Lewis Research Center
Cleveland, Ohio 44135–3191

8. PERFORMING ORGANIZATION REPORT NUMBER

E–8277

9. SPONSORING/MONITORING AGENCY NAME(S) AND ADDRESS(ES)

National Aeronautics and Space Administration
Washington, D.C. 20546–0001

10. SPONSORING/MONITORING AGENCY REPORT NUMBER

NASA TM–106435
AIAA–94–0865

12a. DISTRIBUTION/AVAILABILITY STATEMENT	12b. DISTRIBUTION CODE
Unclassified - Unlimited Subject Category 07	

13. ABSTRACT (Maximum 200 words)

A production 3-D elliptic flow code has been used to calculate non-reacting and reacting flow fields in an experimental mixing section relevant to a rich-burn/quick-mix/lean-burn (RQL) combustion system. A number of test cases have been run to assess the effects of the variation in the number of orifices, mass flow ratio and rich-zone equivalence ratio on the flow field and mixing rates. The calculated normalized temperature profiles for the non-reacting flow field agree qualitatively well with the normalized conserved variable isopleths for the reacting flow field indicating that non-reacting mixing experiments are appropriate for screening and ranking potential rapid mixing concepts. For a given set of jet momentum-flux ratio, mass flow ratio, and density ratio (J, MR, and DR), the reacting flow calculations show a reduced level of mixing compared to the non-reacting cases. In addition, the rich-zone equivalence ratio has noticeable effect on the mixing flow characteristics for reacting flows.

14. SUBJECT TERMS			15. NUMBER OF PAGES
Dilution; Jet mixing flow; Gas turbine; Combustion chamber; Emissions			28
			16. PRICE CODE A03

17. SECURITY CLASSIFICATION OF REPORT	18. SECURITY CLASSIFICATION OF THIS PAGE	19. SECURITY CLASSIFICATION OF ABSTRACT	20. LIMITATION OF ABSTRACT
Unclassified	Unclassified	Unclassified	

National Aeronautics and
Space Administration

Lewis Research Center
21000 Brookpark Rd.
Cleveland, OH 44135-3191

Official Business
Penalty for Private Use $300

POSTMASTER: If Undeliverable — Do Not Return

	NAME	DATE	MS
DO NOT REMOVE SLIP FROM MATERIAL Delete your name from this slip when returning material to the library.	Kyu. C. Hwang	3/14/95	219

RIAD N-75

NASA Langley (Rev. Dec. 1991)